8-2011

Using slow-release permanganate to remove TCE from a low permeable aquifer at a former landfill

Mark D. Christenson
University of Nebraska-Lincoln, mdchristenson@huskers.unl.edu

Using slow-release permanganate to remove TCE from a low permeable aquifer at a former landfill

By

Mark D. Christenson

A THESIS

Presented to the Faculty of

The Graduate College at the University of Nebraska

In Partial Fulfillment of Requirements

For the Degree of Master of Science

Major: Natural Resource Sciences

Under the Supervision of Professor Steve Comfort

Lincoln, Nebraska

August, 2011

Using Slow-Release Permanganate to Remove TCE from a Low Permeable Aquifer at a Former Landfill

Mark Christenson, M. S.

University of Nebraska, 2011

Advisor: Steve Comfort

Past disposal of industrial solvents into unregulated landfills is a significant source of groundwater contamination. In 2009, we began investigating a former unregulated landfill with known trichloroethene (TCE) contamination. Our objective was to pinpoint the location of the plume and treat the TCE using in situ chemical oxidation (ISCO). We accomplished this by using electrical resistivity imaging (ERI) to survey the landfill and map the subsurface lithology. We then used the ERI maps to guide direct push groundwater sampling. A TCE plume (100-600 μg L^{-1}) was identified in a low permeable silty-clay aquifer (K_h = 0.5 m d^{-1}) that was within 6 m of ground surface and underlain by an even lower permeable zone (K_h = 0.04 m d^{-1}). Because injecting a liquid oxidant into the low permeable aquifer would have been difficult, we manufactured slow-release potassium permanganate candles (SRPCs) to treat the TCE. SRPCs were prepared by heating and mixing $KMnO_4$ and paraffin wax at a 4.6 to 1 ratio (w/w), and then pouring the heated mixture into circular

cardboard molds (91.4 cm long) that were either 5.1 cm (2 in) or 7.6 cm (3 in) in diameter. For comparison, we inserted equal masses of SRPCs (7.6-cm vs 5.1-cm diameter) into a low permeable aquifer (4.6 m vertical thickness) in staggered rows that intersected the TCE plume. The 5.1-cm diam candles were inserted directly into the formation using direct push hollow rods at 21 locations. The 7.6-cm SRPCs were encased in slotted containers and placed in 10 permanent wells. Pneumatic recirculators that emitted small air bubbles were placed below the 7.6-cm SRPCs in the second year to facilitate permanganate distribution. Results obtained prior to inserting recirculators showed a 64 to 82% reduction of TCE in the 7.6-cm candle treatment zone after 342 d and between 64 to 100% decrease in associated ethene degradates. These results support using slow-release permanganate candles as a means of treating chlorinated solvents in low permeable aquifers.

Acknowledgements

I would like to thank my advisor, Steve Comfort, for his guidance, knowledge, and assistance throughout my graduate experience. I would also like to thank Ed Harvey for his advice and support during my educational endeavors. Additionally, I want to thank Yusong Li for her theoretical expertise and modeling prowess. I can also not forget to show Nat, Tiger, and Ann my appreciation for all of their help in the field and the laboratory.

I would like to express immense gratitude toward Matt Marxsen and Travis Porter of the University of Nebraska Conservation and Survey Division. Without their support and technical knowledge, our field sampling, well installation, and SRPC installations would not have been possible. I would also like to thank Dr. Todd Halihan of Oklahoma State University and Stuart McDonald and Reed Terry of Aestus LLC, for their generous intellectual and technical assistance during our electrical resistivity imaging. Additionally, I would like to thank Napatsawan “May” Noiwong for her assistance with the GIS plume contouring.

Lastly I would like to give my sincerest thanks to my wife, Samantha, for her infinite patience and helping hand to take care of our family and household throughout my entire education. I would also like to thank my daughter Zoe for “uncomplainingly” letting me take time away from her while I worked on this thesis, and to apologize for not taking her fishing for the last two years.

Preface

This thesis is written in a journal submission format. Chapter 1 consists of an introduction and a literature review on the subject of chlorinated solvent contamination and remediation using oxidative treatments. Subsequently, Chapter 2 reports the objectives and hypothesis of the thesis, materials and methods, results, and conclusions of the research. Appendix A provides supplemental information to the main body of the thesis in Chapter 2. Finally, Appendices B-H provide information from additional studies done in support of the research and propose future work in the field.

Table of Contents

List of Tables

List of Figures

CHAPTER 1. Literature review

1. Introduction

One of the most prevalent threats to groundwater quality is contamination from chlorinated solvents. Chlorinated solvents were first produced in Germany in the nineteenth century and in the U.S. in 1906. Manufacturing industries began using chlorinated solvents in earnest during WWII and increased usage dramatically over the next three decades (Pankow and Cherry, 1996). Chlorinated solvents were traditionally used as degreasers, preservatives, and chemical intermediates. Among the many chlorinated solvents produced, dichloromethane, trichloroethene, tetrachloroethene, and 1,1,1-trichloroethane are undoubtedly among the top 10 organic groundwater pollutants worldwide (Schwarzenbach et al., 1993). Other common chlorinated solvents include chloroform and carbon tetrachloride. The reason chlorinated solvents are such an environmental concern is that the chemical attributes that made them desirable for industrial uses have also made them difficult to detect and remove from soil and water. These chemical attributes include: (i) high volatility that allows them to move as vapor plumes in soils; (ii) chemical stability under aerobic conditions (i.e., highly persistent); (iii) slightly soluble in water, which means small releases can contaminated large volumes of groundwater; (iv) densities greater than water, which allows them to seep deep underground; and (v) low viscosity, which allows rapid movement through porous media.

For clarity, other terms often used to describe chlorinated solvents include dense nonaqueous phase liquids and volatile organic compounds. Because chlorinated compounds have densities greater than water, they have also been termed dense nonaqueous phase liquids (DNAPLs). It should be noted that many compounds besides chlorinated solvents are considered DNAPLs such as pesticides, substituted aromatics, and other halogenated organics. Volatile organic compounds (VOCs) are compounds that have a high vapor pressure and low water solubility. Some chlorinated solvents are also considered VOCs and include trichloroethene and tetrachloroethene as well as their common degradation products (1,1-dichloroethene, *cis*-1,2-dichloroethene, *trans*-1,2-dichloroethene and vinyl chloride).

From a public perspective, a fundamental problem associated with chlorinated solvents is that many are classified as actual or potential cancer-causing agents and therefore have stringent drinking water standards. The Safe Drinking Water Act has stipulated that the maximum contaminant levels (MCLs) for many chlorinated solvents is at or below 5 μg L^{-1} (ppb). Therefore, just one liter of trichloroethene (TCE) for example, could theoretically contaminated 50 million gallons of water.

Chlorinated solvents were often released into the soil or groundwater as a liquid that was immiscible with and denser than water. DNAPLs are pulled downward through soil pores by gravity (Fig. 1). Initially, DNAPL displaces air and/or water from the pore space. As the DNAPL migrates it often leaves a trail of residual blobs or ganglia held in place by capillary forces. DNAPL can

form continuous pools, frequently on top of low permeability layers. Where DNAPL is present, constituents will dissolve into water, sorb to solids, and partition to soil gas. Thus, managing and remediating chlorinated solvents requires an understanding of the equilibrium partitioning that occurs between the chlorinated solvents present in the dissolved phase, sorbed to solids and in the gas phase (Sale et al., 2007).

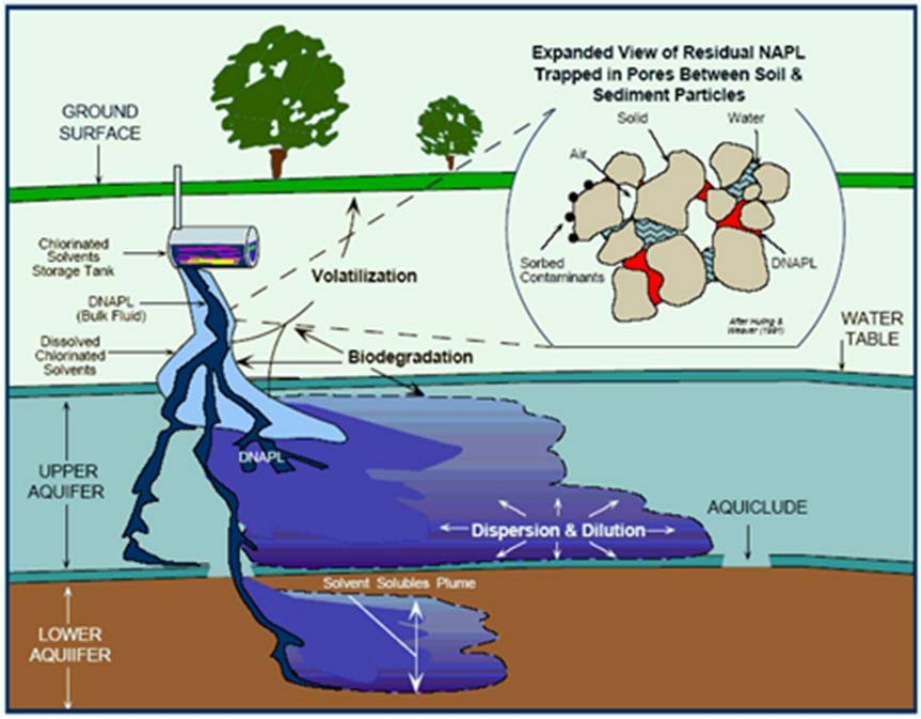

Figure 1.1. Transport of DNAPL
(Source http://oceanworld.tamu.edu/resources/oceanography-book/Images/DNAPL.gif)

Today the number, size and persistence of chlorinated solvent sites have created an enormous environmental problem. There are an estimated 15,000 to 25,000 chlorinated solvent sites in the U.S. with groundwater plumes that

range from 500 to 5000 ft. The plumes that have been observed today were likely caused by releases that occurred in the 1960's through the 1980's (Sale et al., 2007). The types of field sites often contaminated with chlorinated solvents include previously identified hazardous waste sites, military defense sites, and dry cleaning facilities. The United States Environmental Protection Agency (USEPA) has found TCE at more than 1,500 hazardous waste sites that are being regulated under the Comprehensive Environmental Response, Compensation, and Liability Act (CERCLA) and the Resource Conservation and Recovery Act (RCRA). More than 3,000 Department of Defense sites are known to be contaminated with TCE and/or perchloroethene (PCE) (Stroo et al., 2003) and as of 2002, between 25,000 and 35,000 dry cleaning businesses were operating in the United States (Lohman, 2002). Thus, the number of known TCE contamination sites coupled with the potential for new sites at dry cleaning or industrial/manufacturing facilities presents a daunting challenge to engineers, scientists, and policy makers.

Spills of chlorinated solvents in aquifers are exceptionally difficult to clean up. At many sites, plumes have tainted water supply wells at concentrations above the MCLs for drinking water. At each site where DNAPLs have contaminated the local groundwater, there are two major components to the problem: a subsurface source zone and a groundwater plume. Usually, most of the contaminant mass is in the source zone, but the tainted plume usually occupies a much larger volume of the aquifer. Thus, unless most of the source is removed (i.e., >99.9%), permanent aquifer restoration to drinking water

standards will not be achievable in the short term. While numerous conventional pump-and-treat (P&T) facilities have been installed to treat these sites, P&T facilities have enormous operating expenses and offer no short-term solutions. Simple excavation is also not practical because of the depths to which it is possible for DNAPL to have moved.

New technologies being developed for source-zone remediation are of two-types, those that bring the contaminant mass to the surface for treatment or disposal (pump and treat) and those that treat the source zone in situ. In situ treatments can be categorized into physical, chemical, and biological approaches. Several types of chemical treatments have been developed and applied to the subsurface. Commonly used chemical treatments include: direct chemical oxidation, direct chemical reduction, secondary reduction or oxidation, and metal-enhanced dechlorination. Direct chemical oxidation involves injecting chemical oxidants such as hydrogen peroxide (with ferrous iron), permanganate (sodium or potassium), perchlorate, persulfate, and ozone (Watts, 1998). Direct chemical reduction uses reducing agents like sodium dithionite. Secondary reduction or oxidation occurs when injected chemicals influence the oxidation-reduction potential of the aquifer, which subsequently induces transformation of the contaminant. Metal-enhanced dechlorination typically involves the use of zerovalent iron in either granular or colloidal form.

Over the past two decades one method that is relatively mature and frequently used for treating chlorinated ethenes is in situ chemical oxidation (ISCO) with permanganate. The kinetics and mechanisms of chlorinated

solvent oxidation by permanganate are well known (Vella and Veronda, 1992; Schnarr et al., 1998; Yan and Schwartz, 2000; Siegrist et al., 2001; Li and Schwartz, 2004a). The stoichiometry of the MnO_4^--TCE oxidation reaction is reported by many sources and is described in Equation 1 (Schnarr et al., 1998; Li and Schwartz, 2004a; Siegrist et al., 2001).

$$C_2Cl_3H + 2MnO_4^- \rightarrow 2CO_2 + 2MnO_2(s) + 3Cl^- + H^+ \quad (1)$$

Using permanganate for ISCO treatment of TCE offers numerous advantages such as the complete destruction of TCE and the production of innocuous products (primarily CO_2, Cl^-, and MnO_2) (Vella and Veronda, 1992; Sra, 2010). Permanganate is highly soluble making it possible to apply high concentrations while minimizing solution volumes. Additionally, the rapid rate of the reaction, low cost of permanganate, and ease of application makes ISCO with permanganate a very attractive option (Lee et al., 2008b).

One of the major challenges to implementing ISCO in the field environment is ensuring contact between permanganate and the chemical of concern. This challenge exist both spatially and temporally. The difficulty in achieving adequate oxidant distribution has been recognized since some of the earliest field applications of permanganate (Schnarr et al., 1998). Heterogeneity in the subsurface often leads to bypassing of dissolved phase contaminants in low permeable zones (Siegrist et al., 2001). Additionally, temporal distribution difficulties can be seen after permanganate flushing or injections are discontinued and back-diffusion from low permeable zones creates a rebound effect causing contaminant concentrations in monitoring

wells to increase (Sale et al., 2007). Thus, the need to develop long-term remedial options that could treat large contaminant plumes in various geologies has been the focus of much research in the field of ISCO.

2. Slow-release permanganate

A challenge to successfully implementing ISCO is when the contaminants are present in low permeable aquifers. Most ISCO treatments to date have involved injecting oxidants into aquifers as liquids. A common problem with any chemical injection however, is that some sites may have finer textured soils that do not readily accept liquid injections. When this occurs, the chemical oxidant can be observed coming back out of the injection borehole because it offers the path of least resistance. Difficulty in addressing contamination in low permeability soils may be alleviated to some degree by taking a passive approach where a controlled-release oxidant is inserted into the formation and allowed to dissolve and intercept the contaminants over many years.

Recent efforts to address the ISCO challenges imposed by heterogeneity in the subsurface and low permeable aquifers have focused on developing technologies that could supply a continuous input of permanganate into a contaminated aquifer for months to years. Ideally this new form of ISCO would be a passive system utilizing a reactive barrier that could treat dissolved contaminant and/or dense non-aqueous phase liquid migration (Ross et al., 2005; Lee and Schwartz, 2007a; Swearingen and Swearingen, 2008). The inspiration for such technologies was primarily taken from the pharmaceutical

and agricultural industries that have been conducting research in the field of slow release drugs, fertilizers, and pesticides.

Research into slow-release permanganate (SRP) has led to the creation of two basic forms. The first form of SRP was created by encapsulating a core of either individual or multiple $KMnO_4$ granules in an organic polymer shell (Kang et al., 2004; Ross et al., 2005). The shell material was generally comprised of straight waxes, chlorinated waxes, and/or resins (Kang et al., 2004; Ross et al., 2005). Encapsulation was achieved by either a molten suspension and cooling (MSC) method (Kang et al., 2004) or a spinning disk method (Ross et al., 2005). One advantage of the spinning disc method is the ability to vary the rate of the spinning disk, thereby, changing the size of the encapsulated SRP. Kang et al. (2004) reported a mean encapsulated permanganate particle diameter of 874 (±377) μm with the MSC method, while Ross et al. (2005) were able to achieve encapsulated permanganate particles with diameters ranging from 60 to 2000 μm in a more controlled fashion. The ability to control SRP size is important because it influences both the feasibility of SRP delivery in situ, as well as the life expectancy of the SRP.

The second form of SRP, and one that has received more attention, is monolithic pellets consisting of permanganate granules suspended in a polymer matrix. This form of SRP utilizes similar wax and resin polymers. The molten polymer and $KMnO_4$ mixtures are molded into cylindrical pellets 2.5 to 5 cm in diameter and ranging from 10 cm to 1.5 m in length (Lee and Schwartz, 2007a,b; Lee et al., 2008a,b; Lee et al., 2009). Additionally, the latest

generations of SRP have included a silica sand amendment in the polymer matrix (Lee et al., 2008b).

The justification for the two types of SRP is directly related to the intended delivery strategy. Encapsulated particle type SRP is primarily intended to be delivered via pressurized direct push injection (Siegrist et al., 1999; Ross et al., 2005). Thus, the particles must be sufficiently small to avoid clogging of the injection equipment. The principal disadvantage of small sized encapsulated particles is their shortened life expectancy due to limited mass. Conversely, monolithic type SRP is intended to be placed into a contaminated aquifer via traditional well systems, and may offer the advantage of a longer life span (Lee and Schwartz, 2007a). The disadvantage of the monolithic SRP is that this strategy requires a more cumbersome traditional well-based delivery system that is likely to be more time consuming, invasive, permanent, and costly.

The most recent forms of SRP have utilized paraffin wax as the polymer of choice. There are a number of factors which make paraffin a desirable component for SRP. Paraffin is solid at room temperature yet has a relatively low melting point which makes it easier and safer to handle and requires less energy during SRP manufacturing. Another very important property of paraffin is its insolubility in water and high solubility in organic solvents. The solubility characteristics of paraffin act to shield $KMnO_4$ from water while at the same time sorbing organic contaminants from the aqueous phase (Kang et al., 2004; Ross et al., 2005). Paraffin is also environmentally benign, and is biodegraded readily by such microorganisms as *Pseudomonas*, *Mycobaterum*, *Nocardia*,

Corynebacterium, and *Micrococcus* (Kang et al., 2004). Hence, there should be little concern for contamination from paraffin wax remaining in the aquifer after SRP systems are spent of $KMnO_4$. Paraffin and $KMnO_4$ are non-reactive, thus there is no consumption of permanganate by the polymer matrix (Kang et al., 2004). Additionally, paraffin wax is inert, inexpensive, and readily available making it an ideal constituent for large scale production of SRP (Kang et al., 2004; Ross et al., 2005).

2.1 Release kinetics

The fundamental advantage of SRP over traditional liquid injection is the ability to slowly release oxidant over months to years. Characterizing the release kinetics is rather challenging due to the desired length of service and variability in SRP design and manufacturing. While quantifying long term SRP performance is difficult to achieve due to the length of experiments that would be required to gain observable data, the mechanisms by which permanganate is released from the SRP matrix at early times has helped to predict how different SRP designs will perform.

After contact with water, the granules of $KMnO_4$ exposed at the surface of the SRP rapidly dissolve. This results in a large spike in the mass flux of permanganate from the SRP (Lee and Schwartz, 2007a). As the $KMnO_4$ granules continue to dissolve the surface of the exposed granules retreats further into the SRP, consequently creating secondary porosity within the polymer matrix (Kang et al., 2004; Lee and Schwartz, 2007b). It is diffusion of the dissolved permanganate through the newly formed matrix pores that then

dictates the release rate from the SRP. As a result, the further the dissolution front retreats from the exterior of the SRP, the longer the diffusion pathway becomes, and hence, the slower the SRP releases permanganate (Lee and Schwartz, 2007b).

As described above, the release of permanganate from the SRP matrix is fundamentally a dissolution-diffusion process (Kang et al., 2004; Ross et al., 2005; Lee and Schwartz, 2007a). Because permanganate will likely never reach its solubility limit (≈60 g L-1) the dissolution rate will vary only with groundwater temperature. Therefore, Lee and Schwartz (2007a) concluded that diffusion is the rate controlling mechanism that controls permanganate release. Lee and Schwartz (2007a) calculated an effective diffusion coefficient (D_e) of 8.61×10^{-7} cm^2 s^{-1} based on observed permanganate release from a pre-rinsed 2.5 cm x 5 cm (ID x length) SRP pellet containing 32.2 g $KMnO_4$ in flowing water over 20 d (Eqn. 2).

$$\frac{dQ}{dt} = -2\pi h D_e r \frac{dC}{dr} \quad (2)$$

Where Q is the quantity of permanganate released, h and r are the height and the radius of the dissolution front, t is time, D_e is the effective diffusion coefficient and C is the concentration of permanganate in the SRP pellet. As the D_e decreases, release rates from the SRP pellet will also decrease. Thus, changes in the ratio of permanganate to polymer and the initial mass of $KMnO_4$ loaded will have the greatest effect on D_e, and will subsequently dictate the release characteristics of the SRP (Lee and Schwartz, 2007b).

Two kinetics models have been proposed to describe the release of permanganate from SRP pellets. Kang et al. (2004) tested zero-order, modified first-order, modified hyperbola, and the Sinclair/Peppas models. They found that their permanganate release data best fit ($r^2 > 0.974$) the Sinclair/Peppas model (Eqn. 3).

$$Q = kt^n \tag{3}$$

Where Q is the fraction of $KMnO_4$ released at time t, k is the release constant unique to the SRP, and n is a diffusional exponent which increases as the ratio of $KMnO_4$ to polymer increases (Kang et al., 2004). This model predicted SRP mixed at a 1:1 ratio (w/w) of wax to permanganate and having an average spherical diameter of slightly less than 1 mm would take as long as 1.7 months to release 90% of the permanganate (Kang et al., 2004).

The other model most commonly used to describe release kinetics was a first-order decay model (Ross et al., 2005; Lee and Schwartz, 2007a,b). This behavior results from an increase in diffusion path length caused by the retreat of the dissolution front into the interior of the SRP (Lee and Schwartz, 2007b). Based on the D_e calculated during early column experiments, Lee and Schwartz (2007b; 2008b) developed a numerical finite-difference model that coupled with data from flow tank studies predicted release rates of 2.5 kg d^{-1} at 1 d, 22 g d^{-1} at five years and 12 g d^{-1} at ten years from SRP with an original mass of 198 kg $KMnO_4$. Additionally, they found concentrations of permanganate ranged between 0.5 and 6.0 mg L^{-1} during a 42 d test.

2.2 Contaminant destruction efficiency

Generalizing contaminant destruction efficiencies from SRP can be difficult due to the wide variability in SRP characteristics and applications (i.e. size and shape, manufacturing process, permanganate loading, delivery system, permanganate release characteristics, and treatment zone distribution). Likewise, the above factors do not take into consideration traditional hindrances to ISCO (aquifer heterogeneity, natural oxidant demand, low permeable media, contaminant concentrations, etc.). Thus, until forms of SRP become more consistent it may be difficult to make direct comparisons between researchers' results. Nonetheless, a few generalizations can be made about contaminant destruction that may be helpful.

First, contaminant destruction occurs rapidly shortly after introduction of SRP into the soil-water media because this is when rapid $KMnO_4$ release is observed (Ross et al., 2005). Batch studies of TCE with SRP showed that 70% to 90% of the TCE was initially transformed (3 to 6 d) and this occurred faster than predicted based on permanganate release rates. However, removing TCE below detection limits took longer than expected indicating a need for more sophisticated models for predicting early and late release rates from the SRP (Ross et al., 2005).

Second, oxidation of contaminants by permanganate in the aqueous phase is not the only pathway by which contaminant destruction occurs. As previously noted, one reason for using paraffin wax as the matrix polymer is its high solubility in most organic solvents. Consequently, as permanganate is

dissolving and diffusing out of the SRP, organic contaminants are diffusing into the SRP through the polymer and reacting with encapsulated $KMnO_4$ (Kang et al., 2004; Ross et al., 2005). This behavior was first observed by Ross et al. (2005) when decreases in TCE concentrations were higher than increases in oxidation daughter products (MnO_2 and Cl^-). Further investigations led them to believe that TCE and/or daughter products were sequestered within the SRP. This is likely the reason they observed a faster than expected initial TCE destruction rate and slower than expected oxidation of TCE as determined from mass balance calculations.

Third, limitations of contaminant destruction can be primarily attributed to problems associated with ensuring contact between the contaminant and the oxidant. Removal efficiencies of TCE in a pilot scale tank study of 110 SRP pellets in three discrete barriers yielded destruction rates of TCE ranging between 63% to 67% (172 μgL^{-1}) and 72% to 75% (87 $\mu g\ L^{-1}$) (Lee et al., 2009). They postulated three reasons for the incomplete TCE destruction: 1) insufficient MnO_4^- supply, 2) insufficient residence time of TCE with MnO_4^-, and 3) insufficient mixing of TCE-contaminated water with MnO_4^-. After ensuring a sufficient quantity of MnO_4^- was present and determining a residence time of 405 half-lives within the PRB it was concluded that insufficient lateral transport was the main reason for incomplete TCE destruction (Lee et al., 2009).

3. Permanganate distribution

One of the major challenges facing SRP technologies is improving horizontal and vertical distributions of permanganate within the treatment zone.

With respect to a PRB approach, the more significant challenge is improving the transverse spreading of permanganate so as to fill gaps between SRP delivery points and create what has been called a “closed-gap” treatment zone (Lee and Schwartz, 2007a,b; Lee et al., 2008a,b; Lee et al., 2009). Of course, the ability of the permanganate to migrate laterally is highly dependent upon the specific hydrogeologic conditions of each study site. Nonetheless, in most instances the primary mode of transport transverse to the direction of groundwater flow will be via dispersion. However, dispersion will be less important when groundwater flow rates and particle size distributions are reduced, as is typical in low permeable media such as silts and clays, and diffusion will become more significant (Fetter, 1999).

Because dispersion will dominate in lateral permanganate transport, the effective treatment zone of a PRB may actually be beyond the boundaries of the PRB (Lee et al, 2008a). This has two important implications. First, effective monitoring of PRB performance can only be achieved within, or more appropriately, beyond the boundaries of the closed-gap treatment zone. Samples taken from monitoring wells placed before the closed-gap treatment zone may not be sufficiently mixed to provide proper indication of contaminant destruction efficiency (Lee et al., 2009). The second implication is that as the treatment zone is extended further beyond the PRB the losses of permanganate via oxidation of natural organic matter will increase, thereby, reducing the efficiency of the SRP system (Lee et al., 2009). Thus, any field implementation of well based SRP must take into consideration the lateral and

axial permanganate well spacing, as well as, the axial monitoring well spacing in relation to the PRB.

As previously stated, the axial length of permanganate travel required to close the inter-well gap will be highly dependent upon the site hydrogeology. This can be addressed to a reasonable degree by adjusting the injection point spacing, with the caveat that there are going to be limits on how close direct push and/or traditional wells can be placed in relation to one-another (Lee et al., 2008a). A simple approach to overcoming the spacing problem is to use multiple transects of SRP in a staggered pattern to reduce the magnitude of the inter-well gap (Lee et al., 2009). Alternatively, more complex flushing systems could increase transverse distribution of permanganate. A cyclical injection and withdraw doublet model, described by Lee et al. (2008a), increased lateral distribution and mixing down-gradient from a SRP-PRB after 42 d and maintained the distribution for an additional 50 d via modeling. While field implementation of such a flushing system may be effective, it negates one of the primary advantages of a SRP system; simplicity.

In addition to complications from insufficient lateral mixing, vertical permanganate distribution problems may arise in certain applications of SRP. Specifically, well based delivery systems may experience sinking MnO_4^- within the well's water column (Lee et al., 2008b). Concentration differences of 1 to 20 mg L^{-1} compared to 1 to 6 mg L^{-1} were noticed across as little as 0.5 meter (Lee et al., 2008b). This phenomenon could lead to decreasing contaminant destruction efficiency at shallower depths due to lower MnO_4^- concentrations.

Furthermore, the potential also exists for a significant mass of MnO_4^- to sink out the bottom of SRP wells and end up below the intended treatment zone.

4. Future work

A potential adverse side effect of ISCO with permanganate is the formation and subsequent pore clogging by MnO_2(s), a reduction product of MnO_4^-. The development of a crust or rind at the interface of DNAPL and oxidant, as well as, changes in the local flow regime have been observed (Li and Schwartz, 2002; Li and Schwartz, 2004b). Rinds act to reduce the interfacial area between the oxidant and pure phase thereby reducing contaminant destruction efficiencies (Crimi and Siegrist, 2004). Rind formations also reduce the interfacial area between the pure phase pool and the groundwater, which reduces the mass transfer between the pure and aqueous phases (Crimi and Siegrist, 2004). Subsequently, there are reduced concentrations of contaminants in the aqueous phase and this facilitates the migration of oxidant out of the treatment zone where it can be consumed by natural organic matter. By conducting 2-D experiments with divergent heterogeneous media, Li and Schwartz (2004b) clearly showed the buildup of MnO_2 at the transition boundary between high and low hydraulic conductivity regions. Treatment within these low permeable zones has been a significant hurdle in the field of ISCO for some time, and the added complication of this filtering effect at hydraulic conductivity transition zones only amplifies the problem. Therefore, applications of SRP, intended to last from months to

years, should take into consideration the potential for bypassing due to MnO_2 pore clogging within the treatment zone.

Recent efforts to address pore clogging have focused on preventing the formation of large MnO_2 agglomerates. Use of polymeric phosphates for reducing agglomerate size to increase mobility of MnO_2 has yielded positive results. Using sodium hexametaphosphate (HMP) amendments (5:1 $KMnO_4$:HMP) in oxidant solutions reduced MnO_2 deposition by 85% in iron-rich soils and 53% in clay-rich soils (Crimi et al., 2009). During these same column experiments, flow was completely restricted during flushing of the contaminant zones with oxidant alone. A second major strategy is to dissolve MnO_2 agglomerates after they formed within the treatment zone. Li and Schwartz (2004a,b) accomplished this by flushing a DNAPL treatment zone with organic acids (citric or oxalic). Their visual 2-D tank experiments showed complete dissolution of MnO_2 particles throughout the entire treatment zone. Organic acids were selected for treatment over protonated acids, such as nitric acid, due to increased rates of dissolution by a ligand promoted mechanism versus a proton dissolution mechanism (Li and Schwartz, 2004a). However, one complication of using organic acids was that they exerted an oxidant demand on the permanganate. Nonetheless, additions of polymeric phosphates and/or acids to SRP may increase the lifespan of treatment systems by preventing the formation of lower permeable zones (i.e., MnO_2 buildup) at the point of treatment.

Another proposed area for SRP research is the development of dual-layer matrices. Lee and Schwartz (2007b) describe this form of SRP as a modified monolith style pellet having an inner layer with a higher effective diffusion coefficient. Thus, permanganate could be transported more rapidly from the center of the SRP, and the permanganate release rate of the SRP would be governed by the effective diffusion coefficient of the thinner outer layer. Modeling of such a hypothetical SRP form exhibited zero-order kinetics and, therefore, a more constant release rate resulting in an SRP system that could release 1.65 kg of permanganate daily from a proposed 20 m x 20.3 m x 10 m PRB for the duration of 6.6 years (Lee and Schwartz, 2007b). Additionally, permanganate loading within the two layers could be altered to maximize the life expectancy of the SRP pellet (Lee and Schwartz, 2007b).

References

Crimi, M. L., Siegrist, R. L., 2004. Impact of reaction conditions on MnO_2 genesis during permanganate oxidation. J. Environ. Eng. 130, 562-572.

Crimi, M. L., Quickel, M., Ko, S., 2009. Enhanced permanganate in situ chemical oxidation through MnO_2 particle stabilization: Evaluation in 1-D transport systems. J. Contam. Hydrol. 105, 69-79.

Fetter, C., 1999. Contaminant Hydrogeology, 2nd Edition. Upper Saddle River, New Jersey: Prentice-Hall, Inc.

Kang, N., Hua, I., Rao, P. S., 2004. Production and characterization of encapsulated potassium permanganate for sustained release as an in situ oxidant. Ind. & Eng. Chem. Res. 43, 5187-5193.

Lee, B. S., Kim, J. H., Lee, K. C., Kim, Y. B., Schwartz, F. W., Lee, E. S., Woo, N. C., Lee, M. K., 2009. Efficacy of controlled-release $KMnO_4$ (CRP) for controlling dissolved TCE plume in groundwater: A large flow-tank study. Chemosphere 74, 745-750.

Lee, E. S., Schwartz, F. W., 2007a. Characteristics and applications of controlled-release $KMnO_4$ for groundwater remediation. Chemosphere 66, 2058-2066.

Lee, E. S., Schwartz, F. W., 2007b. Characterization and optimization of long-term controlled release system for groundwater remediation: A generalized modeling approach. Chemosphere 69, 247-253.

Lee, E. S., Liu, G., Schwartz, F. W., Kim, Y., Ibaraki, M., 2008a. Model-based evaluation of controlled-release systems in the remediation of dissolved plumes in groundwater. Chemosphere 72, 165-173.

Lee, E. S., Woo, N. C., Schwartz, F. W., Lee, B. S., Lee, K. C., Woo, M. H., Kim, J. H., Kim, H. K., 2008b. Characterization of controlled-release KMnO4 (CRP) barrier system for groundwater remediation: A pilot-scale flow-tank study. Chemosphere 71, 902-910.

Li, X. D., Schwartz, F. W., 2002. Permanganate oxidation schemes for the remediation of source zone DNAPLs and dissolved contaminant plumes. In: Henry S. M., Warner, S. D. (Eds.) Chlorinated Solvent and DNAPL Remediation. Innovative Strategies for Subsurface Cleanup. American Chemical Society Press, Washington, D.C.

Li, X. D., Schwartz, F. W., 2004a. DNAPL remediation with in situ chemical oxidation using potassium permanganate. Part I. Mineralogy of Mn oxide and its dissolution in organic acids. J. Contam. Hydrol. 68, 39-53.

Li, X. D., Schwartz, F. W., 2004b. DNAPL remediation with in situ chemical oxidation using potassium permanganate. II. Increasing removal efficiency by dissolving Mn oxide precipitates. J. Contam. Hydrol. 68, 269-287.

Lohman, J. H., 2002. A history of dry cleaners and sources of solvent releases from dry cleaning equipment. Environ. Forensics 3, 35-58.

Pankow, J., Cherry, J., 1996. Dense chlorinated solvents and other DNAPLs in groundwater: History, behavior, and remediation. Portland, OR: Waterloo Press.

Ross, C., Murdoch, L. C., Freedman, D. L., Siegrist, R. L., 2005. Characteristics of potassium permanganate encapsulated in polymer. J. Environ. Eng. 131, 1203-1211.

Sale, T., Newell, C., Stroo, H., Hinchee, R., Johnson, P., 2007. Frequently asked questions regarding the management of chlorinated solvents in soils and groundwater. Environmental Security Testing and Certification Program (ESTCP). Washington, D.C.

Schnarr, M., Truax, C., Farquahar, G., Hood, E., Gonullu, T., Stickney, B., 1998. Laboratory and controlled field experiments using potassium permanganate to remediate trichloroethylene and perchloroethylene DNAPLs in porous media. J. Contam. Hydrol. 29, 205-224.

Schwarzenbach, R., Gschwend, P., Imboden, D., 1993. Environmental Organic Chemistry. New York, NY: John Wiley & Sons.

Siegrist, R. L., Urynowicz, M. A., West, O. R., Crimi, M. L., Lowe, K. S., 2001. Principles and Practices of In Situ Chemical Oxidation Using Permanganate. Columbus, OH: Battelle Press.

Siegrist, R. L., Lowe, K., Murdoch, L., Case, T., Pickering, D., 1999. In situ oxidation by fracture emplaced reactive solids. J. Environ. Eng. 125, 429-440.

Sra, K. S., 2010. Mobility enhancement of Mn oxide during permanganate oxidation of TCE. Ground Water Monit. R. 1-8.

Stroo, H., Unger, M., Ward, C., Kavanaugh, M., Vogel, C., Leeson, A., Marqusee, J., Smith, B., 2003. Remediating chlorinated solvent source zones. Environ. Sci. Technol. 37, 224-230.

Swearingen, J., Swearingen, L., 2008. Patent No. US 7,431,849 B1, Encapsulated Reactant and Process. United States of America.

Vella, P. A., Veronda, B., 1992. Oxidation trichloroethylene: comparison of potassium permanganate and Fenton's reagent. In: Echenfelder, W. W. (Ed.), Chemical Oxidation Technologies for the Nineties. Technomic Publishing, Lancaster, Basel.

Watts, R. J., 1998. Hazardous wastes: sources, pathways, receptors. New York, NY, John Wiley & Sons, Inc.

Yan, Y. E., Schwartz, F. W., 2000. Kinetics and mechanisms for TCE oxidation by permanganate. Environ. Sci. Technol. 34, 2535-2541.

CHAPTER 2. Using slow-release permanganate to remove TCE from a low permeable aquifer at a former landfill

Abstract

Past disposal of industrial solvents into unregulated landfills is a significant source of groundwater contamination. In 2009, we began investigating a former unregulated landfill with known trichloroethene (TCE) contamination. Our objective was to pinpoint the location of the plume and treat the TCE using in situ chemical oxidation (ISCO). We accomplished this by using electrical resistivity imaging (ERI) to survey the landfill and map the subsurface lithology. We then used the ERI maps to guide direct push groundwater sampling. A TCE plume (100-600 μg L^{-1}) was identified in a low permeable silty-clay aquifer (K_h = 0.5 m d^{-1}) that was within 6 m of ground surface and underlain by an even lower permeable zone (K_h = 0.04 m d^{-1}). Because injecting a liquid oxidant into the low permeable aquifer would have been difficult, we manufactured slow-release potassium permanganate candles (SRPCs) to treat the TCE. SRPCs were prepared by heating and mixing $KMnO_4$ and paraffin wax at a 4.6 to 1 ratio (w/w), and then pouring the heated mixture into circular cardboard molds (91.4 cm long) that were either 5.1 cm (2 in) or 7.6 cm (3 in) in diameter. For comparison, we inserted equal masses of SRPCs (7.6-cm vs 5.1-cm diameter) into a low permeable aquifer (4.6 m vertical thickness) in staggered rows that intersected the TCE plume. The 5.1-cm diam candles were inserted directly into the formation using direct push hollow rods at 21 locations. The 7.6-cm SRPCs were encased in slotted containers and placed

in 10 permanent wells. Pneumatic recirculators that emitted small air bubbles were placed below the 7.6-cm SRPCs in the second year to facilitate permanganate distribution. Results obtained prior to inserting recirculators showed a 64 to 82% reduction of TCE in the 7.6-cm candle treatment zone after 342 d and between 64 to 100% decrease in associated ethene degradates. These results support using slow-release permanganate candles as a means of treating chlorinated solvents in low permeable aquifers.

1. Introduction

Prior to 1993, small publicly operated landfills in Nebraska were specifically exempt from most solid waste regulations. For example, small landfills were not required to have liners, conduct groundwater monitoring, or take appropriate steps to prevent the public from disposing of used solvents. Although this original exemption was intended to limit the financial burden on small communities, the consequences of not requiring preventative actions have resulted in widespread groundwater contamination. Local communities are now strapped with the financial costs of removing industrial solvents such as tetrachloroethene, trichloroethene, and 1,1,1-trichloroethane chemicals from their groundwater. Traditional remediation techniques such as pump and treat usually require significant capital to construct, are expensive to operate and maintain, and typically must be operated for decades.

An alternative technology that is relatively mature is the injection of liquid oxidants into contaminated aquifers known as in situ chemical oxidation

(ISCO) (Watts and Teel, 2006). Permanganate is widely accepted as an efficient oxidant for ISCO applications and is extremely efficient in mineralizing chlorinated ethenes (i.e., oxidizing to CO_2) (Yan and Schwartz, 1999, 2000). While the chemistry is sound, the application and delivery of permanganate to the contaminants is still a challenge at many sites. Most ISCO treatments to date have involved injecting oxidants into aquifers as liquids. A common problem with any chemical injection however, is that some sites may have finer textured soils that do not readily accept liquid injections. Difficulty in addressing contamination in low permeability soils may be alleviated to some degree by taking a passive approach where a controlled-release oxidant is inserted into the formation and allowed to dissolve and intercept the contaminants over many years. The idea of encapsulating permanganate for sustained release was first proposed several years ago (Kang et al., 2004; Ross et al., 2005; Schwartz, 2005) and since then, a number of publications have documented the efficacy of slow-release oxidant dispersal systems to remove chlorinated solvents at the laboratory-scale and in larger flow-tank systems (Lee and Schwartz, 2007a,b; Lee et al., 2008a,b; Lee et al., 2009).

The former Cozad Solid Waste Disposal Facility is a small community landfill in western Nebraska that operated for twenty years. During this time, unknown quantities of TCE were deposited into the landfill from residential, commercial, and industrial sources. The facility was closed in 1989 after TCE was detected in monitoring wells located down-gradient from the refuse cells at concentrations above the USEPA's Maximum Contaminant Limit (MCL).

Remedial attempts to date have included a dual phase extraction facility, poplar tree plantings to induce phytoremediation, and volatilization ponds. Despite these efforts, TCE contamination remains and the migrating plume has not been contained. Our objective was to pinpoint the location of the plume and implement an in situ chemical oxidation (ISCO) remedial strategy. This was accomplished by using a geophysical approach, which characterized the lithology of the landfill and guided groundwater sampling. Because TCE was found to be located in a low permeable aquifer, we hypothesized that the use of a passive diffusion based treatment strategy using slow-release permanganate candles would be effective at reducing TCE concentrations in the contaminated aquifer. This paper reports the manufacturing and deployment of slow-release permanganate candles (SRPCs) and provides results from both laboratory and field testing aimed at demonstrating the release rates and radius of influence of the SRPCs as well as their efficacy in reducing TCE concentrations.

2. Materials and methods

2.1. Site characterization

To characterize the landfill site and identify the location of the plume, several spatial measurements were made. These included: electrical resistivity imaging (ERI), direct push electrical conductivity logging, hydraulic conductivity measurements and the measurement of soil texture, soil oxidant demand and

groundwater chemistry. Details of these measurements along with chemical standards, and analytical instruments used are provided in Supplementary material (Appendix A, SM- 2).

2.1.1. Electrical resistivity imaging (ERI)

ERI measurements consisted of installing metal stakes (surface electrodes) approximately 15 cm into the ground every 1.5 or 2 m for a total length of either 82.5 or 110 m. The electrodes were attached to a cable and the ERI data was collected with a 56 electrode array using an Advanced Geosciences, Inc., *SuperSting R8* system that induced a current, measured the potential, and stored the data. Data were processed using the Halihan/Fenstemaker processing technique (Halihan and Fenstemaker, 2004). The ERI method measures apparent resistivity with a resolution equal to half the electrode spacing, which in this case was 0.75 or 1 m both horizontally and vertically. ERI imaging depths were 1/5 of the survey line length (16.5 or 22 m).

We collected 22 lines of ERI measurements creating a total of 19 images. Survey locations were based on the locations of: 1) the proposed TCE plume based on existing wells. 2) the refuse cell, 3) phytoremediation plantings, and 4) property lines representing the legal point of compliance. A map of the landfill property and location of ERI lines is provided in Supplementary material (Fig. A1). ERI lines were surveyed using a GPS equipped total station to correct for elevation and to allow fencing of images as displayed in Figure 2.1.

2.1.2 Hydraulic conductivity

Slug tests were conducted near the central portion of the TCE plume (near well C2, Fig. A1) to determine horizontal hydraulic conductivity (K_h). A Geoprobe® GW1600 Pneumatic Slug Test Kit was used to measure isolated water level recoveries at 3, 6, and 10 m. These depths corresponded to the three uppermost ERI layers identified in the ERI survey. We conducted tests in accordance with the GW1600 Standard Operating Procedures (Geoprobe, 2002) with one exception. Rubber electrical tape was used to seal probe rods due to o-ring failures experienced during previous tests at other sites. Slug tests at 3 m (10 ft) and 10 m (32 ft) were conducted in triplicate for two different initial displacements. Due to slow recovery times observed during tests at 6 m (20 ft) we conducted one test at the first displacement and two tests at a second smaller displacement. We used Aqtesolv® aquifer test analysis software and the Bouwer-Rice method for interpreting slug test data in unconfined aquifers to obtain values of K_h (Bouwer and Rice, 1976).

2.1.3 Groundwater chemistry sampling and analysis

A Geoprobe® 6610DT was used to drive an SP16 Groundwater Sampler to desired sample depths. We used a check-ball valve and polyethylene tubing to manually withdraw water from each sample point. When multiple depths were sampled per sampling location, 3 tubing volumes were purged between samples. At each sampling location, we used new tubing and decontaminated the stainless steel screen of the SP16 sampler with deionized

water. Groundwater samples were collected in 40-mL Teflon® septa-capped clear glass vials that contained 0.2 mL of hydrochloric acid preservative.

A YSI® 556 MPS was used to analyze water samples for pH, conductivity, dissolved oxygen, temperature, and oxidation/reduction potential. Because groundwater samples were manually obtained with a check valve and tubing, water was immediately analyzed in a calibration cup rather than utilizing a flow-through cell. Groundwater samples were analyzed for VOCs at the University of Nebraska Water Sciences Laboratory on an Agilent Technologies® 6890N gas chromatograph/mass spectrometer using EPA methods 8260B and 5030C. VOC concentrations were quantified based upon the percent recovery of a fluorobenzene internal standard added to each sample. Each sample was analyzed for trichloroethene, *cis*-1,2 dichloroethene, *trans*-1,2 dichloroethene, 1,1 dichloroethane, 1,2 dichloroethane, and vinyl chloride.

2.2 Slow-release permanganate candle production

A drying oven (Fisher Scientific®-Isotemp Oven 630F), hot plate (Fisher Scientific®-Isotemp Hot Plate 11-100-49SH), 6-quart electric skillet and a 2-quart ceramic cooker were preheated to 93 ± 5 °C. Straight solid paraffin wax (Peak Candle Supply- IGI 1343A) was melted in an electric skillet and subsequently transferred to a ceramic cooker to be kept melted until ready for use. Approximately 600 g of $KMnO_4$ particles (Carus Corp-RemOx®S) were put into glass mason jars and placed into the drying oven to preheat (93°C) for at least 15 to 20 min. 250 mL of melted wax was added to an aluminum wax

pouring pot and placed on the hot plate. A stand-alone mixer with propeller blade was inserted into the wax, and 600 g of preheated $KMnO_4$ were quickly added to the melted wax. The mixture was stirred at approximately 2000 rpm until all $KMnO_4$ particles were coated with wax. Additional melted wax and/or $KMnO_4$ was added to the mixture to achieve a mixture with a milkshake like consistency that was just barely pourable. The final ratio by mass of $KMnO_4$ to paraffin was on average 4.6 to 1. If the mixture cooled too quickly it was briefly placed back into the drying oven to reheat to 93±5°C. The mixture was then poured into a 7.6 cm (3 in) or 5.1 cm (2 in) by 91.4 cm (36 in) stock cardboard tube (Yazoo Mills®) with a poly tube plug inserted into the bottom. The cardboard tube was gently tamped to remove as much trapped air as possible. Once filled, the candle was set aside to cool vertically at room temperature for at least 12 h.

2.3 Laboratory testing of SRPCs

To quantify permanganate release rates and radius of influence, laboratory experiments were conducted with 1.27 cm lengths of the 5.1 and 7.6-cm diam (disc-SRPCs), as well as, with miniature candles (mini-SRPCs).The miniature candles were prepared in a similar manner to ones used in the field trial but were cast in 0.71-cm diameter molds, 2.38 cm in length. The 5.1 and 7.6-cm disc-SRPCs were sealed on the flat top and bottom with a layer of pure wax to ensure diffusion was in the radial direction only, so results could be scaled to any candle length.

For the mini-SRPCs, we placed individual mini-candles into clear glass jars with 200 mL of deionized water. Sample temperature was maintained at 15°C and room temperature in two separate experiments. Immediately prior to sampling, the solutions were gently swirled to mix. The solution was sub-sampled via pipette every ten minutes for the first hour, hourly for the first four hours, and approximately daily for the remainder of the experiment. Similarly, the disc-SRPCs were placed in 12.5 L of room temperature deionized water and sub-sampled in the same manner as above with the exception that samples were stirred to mix prior to sampling and collected weekly after the first ten weeks. Samples were diluted when necessary, and analyzed on a Hach® DR 2800 Visual Spectrum Spectrophotometer at 525 nm.

To characterize SRPC performance, we determined temporal $KMnO_4$ release rates (Flux, J) and concentration ratio (C_r). Flux was calculated using Eq. 1

$$J = 1/A_{SRPC}\,[(C_{n+1}V - C_nV)/(t_{n+1} - t_n)] \quad (1)$$

where A_{SRPC} = exposed surface area of the cylindrical SRPC, C_{n+1} = concentration of MnO_4^- in solution at time t_{n+1}, C_n = concentration of MnO_4^- in solution at time t_n, V = the volume of the solution, $t_{n+1} - t_n$ = elapsed time between MnO_4^- measurements. Concentration ratio was calculated using Eq. 2

$$C_r = CV/M \quad (2)$$

where C = the concentration of $KMnO_4$ in solution, V = the volume of the solution, and M = the initial mass of $KMnO_4$ in the SRPC (Ross et al., 2005). Plots of both J and C_r versus time were fitted using non-linear regression to a 2-parameter power function with SigmaPlot® scientific analysis and graphing software. The fitted equations were used to project the performance of the SRPCs with time.

2.3.1 Radius of influence

To ensure the gap between SRPCs at the field site would be closed, the permanganate radius of influence achievable through diffusion was estimated. Saturated aquifer material collected from sample cores was cut and packed into a 14 cm x 12.7 cm 2D tank. A steel cylinder slightly larger than the diameter of the mini-SRPCs was pressed into the material to create a pseudo borehole. One mini-SRPC was placed into the bottom of the borehole, sand was poured around the SRPC and the top of the borehole was sealed with bentonite. The saturated tank was then sealed and the diameter of the MnO_4^- diffusion front was visually observed, measured, and photographed daily. Individual photographs were digitally enhanced with Microsoft® Video Editing software (Windows Live Movie Maker) to intensify the color contrast so as to more easily quantify diffusion distances. To estimate the mass of permanganate released from the mini-SRPCs in the 2D tank, a parallel

experiment in H_2O was conducted as described in section *2.3* to determine release rates.

2.3.2 Permanganate distribution from SRPC in sand tank with and without a recirculator

Fine washed sea sand (VWR® CAS No. 14808-60-7) was packed into the same 2D tank described above. A well assembly was fabricated using a 1.6 cm ID x 2.0 cm OD polypropylene tube slotted along 10 cm starting 2.0 cm from the bottom of the assembly. The tube was sealed on the bottom and sheathed in fine mesh polyester fabric. The tank was filled with deionized water and the well assembly was centered on the bottom of the tank. Sand was then poured into the tank and allowed to settle under gravity. After the tank was filled with sand, the entire tank was sonicated for 5 min to remove air pockets. Between tests, the tank and well assembly was unpacked, cleaned, and repacked with new sand.

During recirculator tests air was gently bubbled into the water column and vented out the top of the well. Compressed air, supplied by a PETCO® AC9903 aquarium air pump, was pumped through a 3.2 mm ID x 6.4 mm OD polyethylene tube connected to a sintered diffusion stone at the bottom of the well assembly. Three mini-SRPCs with embedded fishing line were tied to each other and to the diffusion stone to ensure they would remain stationary throughout the experiment. For the non-recirculator test three new mini-SRPCs were suspended at the same depth as the mini-SRPCs in the

recirculator tests. Migration of the MnO_4^- was observed and recorded in 5 minute intervals for the recirculator test and daily for the non-recirculator test.

An additional test was conducted to describe the circulation path of water outside the well assembly caused by the recirculator. The tank was packed in an identical manner as described above and the recirculator assembly was inserted into the bottom of the well. Four separate 1 mL injections of a 1000 mg L^{-1} $KMnO_4$ solution were injected through injection ports at the back of the tank into the sand surrounding the well assembly. Migration of the MnO_4^- was observed and recorded in 2.5 min intervals for a total of 50 min.

2.4 Field testing of SRPCs

Treatment of the entire TCE plume was considered impracticable due to the cost to treat the plume in its entirety. Therefore, we installed a permeable reactive barrier (PRB) of SRPCs perpendicular to the direction of contaminant flow. Location of the PRB was primarily chosen with the intent to intercept the contaminant plume where TCE concentrations were greatest and the plume was narrow and shallow (Fig. A2). Other considerations included choosing a PRB location that was accessible, reasonably level, and up gradient from previously existing monitoring wells.

For comparison, we inserted equal masses of the two SRPC sizes (50 7.6-cm diam vs 105 5.1-cm diam SRPCs) into a low permeable aquifer (4.6 m thickness) in staggered rows that intersected the TCE plume. The 7.6-cm candles were placed on 1.2 m centers in two rows while the 5.1-cm candles were inserted via direct push on 0.91 m centers in three rows (Fig. 2.2)

2.4.1 SRPC installation via direct push

Geoprobe® Probe Rods of 1.5 m x 8.3 cm OD x 6.7 cm ID (5 ft x 3.25 inch OD x 2.625 inch ID) and with an expendable tip without o-rings were inserted into the soil in 1.5 m (5 ft) increments. After each rod was pushed into the ground, 5.1 cm SRPCs were removed from the cardboard molds and inserted into the hollow rods. After a total of 4.6 m (15 ft) of probe rods and candles were inserted, one additional probe rod was attached and pushed into the ground to achieve a total depth of 7 m. Expendable point holders were gently lowered down the hollow probe rods onto the top of the candles. This allowed us to visibly determine that the candles remained in place as the probe rods were raised and removed. After all rods were removed, sand was poured around the candles until the hole collapsed near the water table. Probe holes were then sealed above the candles with bentonite.

2.4.2 SRPC installation into permanent wells

The 7.6-cm SRPCs were removed from cardboard molds and inserted into specially manufactured slotted PVC carrier (Titan Industries Inc., Paxton, NE) (Fig. 2.3A). Each carrier was lowered into a 10-cm diam well with a specially built Candle Insertion Tool (CIT, Fig. 2.3B) attached to a rope. Once the PVC carriers were in place, a locking pin (attached to a second rope) was pulled to release the carrier from the CIT and the CIT was removed from the well. Each permanent well received five 7.6-cm SRPCs that were stacked on top of each other, covering an aquifer thickness of 4.6 m. In year 2, pneumatic

recirculators (Fig. 2.3C) were placed at the bottom of the 7.6-cm SRPCs to improve the distribution of permanganate. A specially designed Candle Removal Tool (CRT, Fig. 2.3D) was also manufactured so that the candle carriers could be removed and the SRPCs monitored and replaced when needed. The CRT was attached to a rope and equipped with a trap door that latched onto the carriage bolt on top of the candle carrier (Fig. 2.3A).

2.4.3 Installation of monitoring wells, sampling and analysis

A series of twelve 5.1-cm diam sampling wells were installed to monitor the efficacy of the PRB (Fig. 2.2). Monitoring wells were installed up gradient, down gradient, and inside the PRB. Up gradient wells were placed 1.8 m away from the leading edge of the PRB. Down gradient monitoring wells were placed 1.2 m from the trailing edge of the PRB. Finally, embedded monitoring wells were centered between candles in the PRBs.

Prior to and after completing the PRB installation, all monitoring wells were sampled for VOCs and groundwater chemistry. A GeoTech® Geopump II peristaltic pump and Viton® tubing were used to sample water 0.3 m below the top of the well screen. Sample water was pumped through a flow-through cell until pH changed by less than 0.1 and conductivity changed by less than 10% over one min. The flow-through cell was then disconnected and VOC samples were collected and quenched with hydrazine (35%) when permanganate was visibly present. This protocol was utilized for all VOC sampling. VOC sampling was conducted at 85 d after PRB installation.

In addition to discrete VOC samplings, spatial changes in conductivity throughout the well screen were measured more frequently. This was done to characterize the diffusion front of MnO_4^- and to reduce cost of monitoring the treatment field for VOCs. A Solinst® TLC meter was used to measure temperature, conductivity, and static water level in each well. Measurements were taken in 0.3 m (1 ft) intervals starting from the static water level. Upon reaching the bottom of the well the probe was left in place and low-flow sampling of MnO_4^- occurred. Conductivity sampling was conducted prior to MnO_4^- sampling to prevent erroneous results from well mixing.

Low-flow MnO_4^- sampling was conducted to complement the conductivity measurements described above. Samples were collected with a peristaltic pump after water quality parameters stabilized (change in pH < 0.1 and change in conductivity < 10%) pumping at a rate of 300 mL min^{-1}. Depths collected were 3.4 m (11 ft), which was 0.3 m (1 ft) below the top of the screen, 5.3 m (17.5 ft) (middle of the screen), and 7.3 m (24 ft) (0.3 m from the bottom of the screen). Additionally, direct push samples were collected at the same depths within 30.5 cm of SRPCs after 354 d. Samples were immediately analyzed or placed on ice and transported to the laboratory for measurement with a Hach® DR 2800 Visual Spectrum Spectrophotometer at 525 nm.

3. Results and discussion

3.1 ERI and site characterization

Two-dimensional inversion modeling of ERI data identified four resistivity regions that were assigned different colors for visual interpretation. These resistivity regions had resistivity measurements (ohms-meter) that ranged from 0 to 7 (orange); >7 to 15 (green); >15 to 35 (blue) and >35 to 95 ohm-m (gray) (Fig. 2.1). The lowest resistivity region (highest electrically conductive region) consisted of a layer beginning at or near the ground surface and was prominent throughout most of the refuse cell (orange layer, Fig. 2.1). Beneath the orange region was a layer with higher resistivity properties, represented in green (Fig. 2.1) that intermittently protruded upward into the orange layer creating some discontinuities. The thickest areas of both the orange and green layers were at the highest elevations, near the refuse cell. These layers then decreased moving south and west toward a floodplain near the property boundaries (Fig. 2.1). Beneath the green layer lay two more electrically distinct layers represented by the blue and gray regions. Both layers vary in thickness throughout the site and the gray layer extends beyond the depth of the ERI images (i.e., >16.5 or 22 m).

We found that the ERI survey, soil core analyses, direct push electrical conductivity logging, and slug tests provided complementary results. For example, when ERI images were overlain with direct push electrical conductivity logs, the ERI color regions and EC values match reasonably well (Fig. 2.1A). EC logging indicated finer sediments in the upper 6 m (20 ft)

followed by a transitional region from 6 to 8.2 m (20-27 ft). Beneath 8.2 m (27 ft) conductivity values were indicative of coarser sediments. Probe speed data also supported EC data by identifying the same transitional point ~7.6 m (25 ft) were finer sediments transitioned to coarser sediments. Analysis of soil cores for texture indicated that the orange and green ERI layers were silt loams but between 3 and 7.6 m there was an increase in silt and a decrease in sand content while clay remained relatively constant. Similar to soil texture, both porosity and bulk density were relatively constant throughout the upper aquifer with an average porosity of 0.413 cm^3 cm^{-3} and bulk density of 1.56 g cm^{-3}; both values are characteristic of a silt loam (Soil Science Society of America, 1986). In relation to ERI layers, we did observe a subtle increase in bulk density from 1.49 g cm^{-3} (orange) to 1.61 g cm^{-3} (green layer).

Despite somewhat similar textures among orange and green ERI layers, slug tests from the upper three ERI layers indicated three distinct hydraulic conductivities (Table 1). The highest K_h was in the blue ERI layer consisting of fine to medium sands as indicated by drilling logs. The average K_h in the blue layer was 20 m d^{-1} (65.59 ft d^{-1}). The lowest K_h was in the green ERI layer. The average K_h in the green ERI layer was 0.04 m d^{-1} (0.144 ft d^{-1}) The orange ERI layer, lying above the green and blue layers, had an average K_h of 0.5 m d^{-1} (1.52 ft d^{-1}). Slug test results reaffirmed what was observed during manual groundwater sampling where the ease of obtaining water samples from the different ERI regions followed the order of: blue (readily obtainable), orange (moderate) and green (difficult).

3.2 Groundwater contamination

Analysis of 146 groundwater samples obtained from 64 sampling locations revealed a distinct relationship between TCE contamination and ERI classifications. Nearly all groundwater samples with detectable TCE (and degradation products) were obtained from the orange ERI layer (Fig. 2.4). It is important to note that not all groundwater samples obtained from the orange ERI layers were contaminated but the majority of samples with detectable TCE were from the orange regions. TCE was only detected in six samples obtained from the green ERI layer. TCE was not detected in any of the blue and gray ERI layers. Thus, in most cases, TCE and its degradation products were located within 6 m of the ground surface (Fig. 2.4). Coupled with the hydraulic conductivity results, we believe that the low permeable zone below the orange region, represented by the green ERI layer, is acting as an aquitard to prevent TCE transport into the underlying sands.

On a mass basis, more degradation products were present than TCE indicating that natural attenuation was occurring. 1,1-DCE and *cis*-1,2-DCE were the most commonly detected degradation products and present at the highest concentrations. A map of the degradation product plumes is present in the Supplementary materials (Fig. A3).

In terms of aerial distribution, TCE and degradation products were found in two areas: 1) the southeast edge of the refuse cell and 2) along a transect extending from the dual phase extraction facility to the southeast (Fig. 2.5). TCE concentrations as high as 58.4 μg L^{-1} were found just outside of the

southeast edge of the refuse cell but the majority of contamination in this area was mostly degradation products (Fig A3). The only TCE detected beneath the cell was at the far southeast corner (11.9 μg L^{-1}). The highest TCE detected at the site was 521 μg L^{-1} immediately south of the dual phase extraction facility. From this high point, TCE values decreased along a southeast transect to below the MCL before reaching the southern property boundary (Fig. 2.5).

3.3 SRPC longevity and radius of influence: Laboratory results

Two important questions regarding the efficacy of using slow release permanganate candles are how long will they last? and what is their radius of influence? To answer these questions, laboratory experiments were performed with mini-SRPCs and 1.27 cm segments of the candles (5.1 and 7.6-cm diam) used in the field (disk-SRPCs). Temporal changes in flux (J) and concentration ratios (C_r) were measured on mini-SRPCs at 15°C and room temperature and disk-SRPC at room temperature. A comparison of fluxes from the mini-SRPCs at two temperatures revealed some differences. As expected there was an initially lower flux at 15°C over the first 10 d. Subsequently, the flux at 15°C remained higher than the flux at room temperature. This difference is attributed to a faster dissolution of permanganate from the surface of SRPCs at room temperature, which subsequently caused diffusion limited release to become the primary release mechanism sooner than at 15°C. Thus, the lower temperature SRPC flux exhibited a lag before diffusion dominated release. It is likely that this lag effect would not be significant on the scale of months or

years. Both the mini and disk SRPCs can be characterized as giving a rapid release of MnO_4^- followed by a more sustained release. Higher initial fluxes were observed with the mini-SRPC versus the disk-SRPCs. This difference is likely related to production where the miniature candles were cast in molds and then pushed out while the 5.1 and 7.6-cm disc-SRPCs were cast in cardboard tubing that was peeled off before use. The act of pushing the miniature candles out of molds (i.e., friction) removed some of the outside wax, which made their initial dissolution rates greater than those observed in the larger candles (5.1 and 7.6-cm diameter).

Several equations have been used to fit dissolution data to predict longevity. Examples include first-order decay (Lee and Schwartz, 2007b) and power function (Kang, et al., 2004). Depending on the equation used, the projected longevity can vary by many years. Attempts at fitting our flux and C_r data to previously used equations also showed considerable variability in projected longevity. For simplicity, we picked two years as a timeframe and then predicted flux and C_r from our disk-SRPCs. Results showed a 20.8 mg d^{-1} flux per 2.54 cm of candle length and C_r equaling 0.195 at 2 yr (Fig. 2.6).

To predict the radius of influence in the field, we inserted mini-SRPC into the low permeable aquifer material (orange ERI region) packed into a 2D tank and then visually measured permanganate distribution. Results showed that within 1 d, the permanganate distribution had a diameter of 3.9 cm (Fig. 2.7). By dividing the permanganate distribution in half and accounting for the radius of the mini-SRPC (0.355 cm), the permanganate had migrated 1.6 cm beyond

the candle after 1 d. We similarly observed this type of behavior when a mini-SRPC was placed inside an intact soil core and saturated overnight (Fig. A4). Subsequent measurements showed radius of influences of 3.7 cm after 7 d, 4.6 cm after 14 d and 5.25 cm after 35 d, the time when the majority of the permanganate had been estimated to be released from the mini-SRPC (Fig. 2.7). Scaling results from mini-SRPCs to field SRPC is not straightforward because both candle size (i.e. diameter) and permanganate mass differ. Given that diffusion rates are dependent on concentration gradients, it is reasonable to assume that the field SRPC will impart a greater radius of influence because they can sustain a higher concentration gradient and should not become mass limiting for years as opposed to days for the mini-SRPCs. Actual diffusions distances will also be highly dependent on soil textures, oxidant demand, and groundwater flow rates.

Ultimately, the maximum transverse distances permanganate must travel through the native aquifer material to close the gaps between the SRPCs used in our field test were 12.7 cm (5.1 cm SRPC) and 17.9 cm (7.6 cm SRPC). In an aquifer with similar hydrogeologic properties to the Cozad aquifer, solid fracture emplaced permanganate diffused to create a reactive zone >20 cm (radius) in 10 mo (Siegrist et al., 1999). Their subsequent diffusion experiments utilizing the same aquifer material yielded a permanganate front migration rate of 0.1 cm d^{-1} over 40 d from a 5000 mg L^{-1} MnO_4^- solution (Struse et al., 2002). When compared with our SRPC radius of influence experiments, factoring out the early time spike in permanganate flux and late

time mass limited flux, we calculate a visible permanganate front mean migration rate of 0.17 cm $d^{-1,}$ which is comparable.

While horizontal permanganate migration away from the mini-SRPCs was encouraging in the low permeable material, we also recognized that the 2D tank differed from the field conditions not only due to packing, but also because the direct push 5.1-cm SRPCs were surrounded by a small volume of sand and the 7.6-cm SRPCs were inserted into wells that were not in immediate contact with the low permeable aquifer material. With regard to SRPCs, the downward migration of permanganate is of greatest concern inside the free water of the injection wells (Lee et al., 2008b). When mini-SRPCs were placed directly in water, we observed a steady stream of permanganate migrating down from the candle. Similar results were observed in a 10% KCl solution (Fig. A5). While density driven flow of permanganate has been reported in the past (Lee et al., 2008b), the chemical structure of $KMnO_4$ also lends itself to intermolecular forces (e.g., dipole-dipole) that are cohesive and cause the molecules to stick together. This cohesiveness can help to exert downward force even in the presence of coarser aquifer material. In 2D tank experiments with sand, we observed uneven permanganate distribution in surrounding media due to sinking of permanganate within the well and out the bottom (Fig. 2.8A). To prevent downward migration, the permanganate molecules need to be separated and solvated so that they can hydrogen bond with H_2O. Consequently, we repeated the 2D tank experiment with a pneumatic recirculator that emitted small air bubbles to physically break

apart the permanganate molecules and for comparison, photographed the migration patterns (Fig. 2.8B).

Visible permanganate migration patterns from the mini-SRPC alone formed a Christmas tree shape typical of permanganate plumes in sandy media. It took 5 d for permanganate to be visible throughout the majority of the tank. It is clear that the permanganate was accumulating at the bottom of the 2D tank, and stacking its way toward the top. Thus, in a theoretical "bottomless" tank the treatment zone surrounding the well assembly may never have become saturated with permanganate.

Conversely, when small bubbles were emitted from the recirculator, an upside-down Christmas tree distribution pattern was observed. Moreover, the time needed to visibly saturate the tank with permanganate was ~75 min, considerably less than the 5 d required without the recirculator. Additionally, the time needed to visibly saturate the treatment zone horizontal to the screened interval was only 30 min, and this was the first section of the tank treated instead of the last as observed without the recirculator. During subsequent injection tests, circulation of water into the bottom of the well and out the top of the well was clearly evident. It was hypothesized that air bubbles injected into the bottom of the well and rising to the surface through the water column created suction at the bottom of the well and discharge at the top. Additional photographs demonstrating this behavior are provided in Supplementary material (Fig. A6).

3.4 SRPC: Field results

Monitoring wells were sampled before SRPC installation, as well as, at 85 d and 342 d after SRPC installation. All wells were sampled with a low-flow sampling technique so as to not artificially accelerate permanganate migration into the monitoring wells. Rather, we wanted the permanganate to diffuse and migrate from SRPCs under natural gradients. Given the low permeability of the aquifer and average linear groundwater velocity (v = 0.42 m yr^{-1}), monitoring wells located 1.2 m down gradient from the SRPCs (S-9-12, Fig. 2.2) are not expected to show treatment effects for a few years. Similar calculations for the monitoring wells embedded within the SRPC (S 5-8) treatment zone (within ~0.5 m of the SRPCs) indicate a travel times of 1.2 yr. This travel time, however, does not account for the chemical diffusion of permanganate away from the SRPCs and the fact that wells and SRPCs were packed with sand and thus provided more transmissive zones. Of the four wells located within the treatment zone (S-5-8), wells S-7 and S-8 showed a 64 to 82% decrease in TCE and between 64 to 100% decrease in associated ethenes at our last sampling (342 d) (Fig. 2.9).

While 2D tank tests showed that permanganate would diffuse horizontally away from the SRPC in low permeable media (Fig. 2.7), our more frequent monitoring of permanganate and electrical conductivity (EC) changes across the well screen with time indicated this may not be occurring with the SRPCs that were placed in permanent wells. EC measurements in well S-7 showed a large spike in EC and permanganate at the bottom of the well screen that

gradually moved toward the surface with time (Fig. A7). To circumvent the possibility of density driven flow, recirculators were placed at the bottom of the 7.6-cm SRPC wells in July, 2011.

4. Conclusions

Investigations at a former solid waste disposal site revealed a dissolved trichloroethene plume in a low permeable aquifer within 6 m of ground surface. To remediate the contaminant plume 91.4 cm long by 5.1 cm OD or 7.6 cm OD slow-release permanganate candles (SRPCs) were manufactured using melted paraffin wax and potassium permanganate. Material costs per candle (91.4 cm long) were approximately $17.50 (5.1-cm) and $39.50 (7.6-cm). Laboratory testing of the SRPCs predicted that they could release >20 mg of permanganate daily per 2.54 cm of length for the first two years of use. The permanganate candles were placed into the aquifer in staggered rows to create a permeable reactive barrier (PRB). Following SRPC installation groundwater sampling of monitoring wells in the 7.6 cm SRPC treatment zone showed a 64 to 82% decrease in TCE at the last sampling (342 d) and between 64 to 100% decreases in associated ethene degradates. Therefore, we believe that slow-release permanganate candles may be used to effectively remove TCE and other chlorinated solvents from low permeable media.

Acknowledgments

The authors greatly acknowledge the technical assistance of the University of Nebraska Conservation and Survey Division. We would also like to thank Dr. Todd Halihan and Aestus LLC, for their intellectual and technical assistance. Additionally, we would like to thank Napatsawan “May” Noiwong for her assistance with the GIS plume contouring. Funding was provided in part by EPA Region 7, Project ER-0635. Partial support was also provided the University of Nebraska School of Natural Resources and Water Center.

References

Bouwer, H., Rice, R., 1976. A slug test for determining hydraulic conductivity of unconfined aquifers with completely or partially penetrating wells. Water Resources Research 12, 423-428.

Geoprobe, 2002. GW1600 Standard Operating Procedures, Technical Bulletin No. 19344. GeoProbe Pneumatic Slug Test Kit. Salina, KS: Kejr, Inc. (February).

Halihan, T., Fenstemaker, T., 2004. Proprietary Electrical Resistivity Imaging Method, 2nd Ed. Oklahoma State University Office of Intellectual Property, Stillwater, OK.

Kang, N., Hua, I., Rao, P. S., 2004. Production and characterization of encapsulated potassium permanganate for sustained release as an in situ oxidant. Ind. & Eng. Chem. Res. 43, 5187-5193.

Lee, E. S., Schwartz, F. W., 2007a. Characteristics and applications of controlled-release $KMnO_4$ for groundwater remediation. Chemosphere 66, 2058-2066.

Lee, E. S., Schwartz, F. W., 2007b. Characterization and optimization of long-term controlled release system for groundwater remediation: a generalized modeling approach. Chemosphere 69, 247-253.

Lee, E. S., Liu, G. M., Schwartz, F. W., Kim, Y. J., Ibaraki, M., 2008a. Model-based evaluation of controlled-release systems in the remediation of dissolved plumes in groundwater. Chemosphere 72, 165-173.

Lee, E. S., Woo, N. C., Schwartz, F. W., Lee, B. S., Lee, K. C., Woo, M. H., Kim, J. H., Kim, H. K., 2008b. Characterization of controlled release $KMnO_4$ (CRP) barrier system for groundwater remediation: a pilot-scale flow-tank study. Chemosphere 71, 902-910.

Lee, B. S., Kim, J. H., Lee, K. C., Bin Kim, Y., Schwartz, F. W., Lee, E. S., Woo, N. C., Lee, M. K., 2009. Efficacy of controlled-release $KMnO_4$ (CRP) for controlling dissolved TCE plume in groundwater: a large flow-tank study. Chemosphere 74, 745-750.

Ross, C., Murdoch, L. C., Freedman, D. L., Siegrist, R. L., 2005. Characteristics of potassium permanganate encapsulated in polymer. Journal of Environmental Engineering, 131, 1203-1211.

Schwartz, F. W., 2005. Semi-passive, Chemical Oxidation Schemes for the Long-term Treatment of Contaminants, The Ohio State University, Columbus, OH.

Siegrist, R., Lowe, K., Murdoch, L., Case, T., Pickering, D., 1999. In situ oxidation by fracture emplaced reactive solids. Journal of Environmental Engineering 125, 429-440.

Soil Science Society of America, 1986. Methods of Soil Analysis, Part 1: Physical and Mineralogical Methods. Madison, WI: American Society of Agronomy, Inc; Soil Science Society of America, Inc.

Struse, A., Siegrist, R., Dawson, H., Urynowicz, M., 2002. Diffusive Transport of Permanganate during In Situ Oxidation. Journal of Environmental Engineering, 128, 327-334.

Watts, R. J., Teel, A. L., 2006. Treatment of contaminated soils and groundwater using ISCO. Pract. Periodical of Haz., Toxic, and Radioactive Waste Mgmt. 10, 2-9.

Yan, Y. E., Schwartz, F. W., 1999. Oxidative degradation and kinetics of chlorinated ethylenes by potassium permanganate. J. Contam. Hydrol. 37, 343-365.

Yan, Y. E., Schwartz, F. W., 2000. Kinetics and mechanism for TCE oxidation by permanganate. Environ. Sci. Technol. 34, 2535-2541.

Table 2.1. Properties of the electrical resistivity layers at the Cozad former solid waste disposal site.

ERI Region	Approximate Depth (meters)	Soil Texture	K_h (ft d^{-1})	K_h (m d^{-1})	Greatest TCE Conc. Observed (µg L^{-1})	Mean Electrical Conductivity (µS cm^{-1})
Orange	0-4	Loess (Silt Loam)	1.52	0.50	521	2225
Green	4-8	Loess (Silt Loam)	0.144	0.04	154	1461
Blue	8-16	Alluvium (Fine-Medium Sand)	65.6	20.0	nd	1103

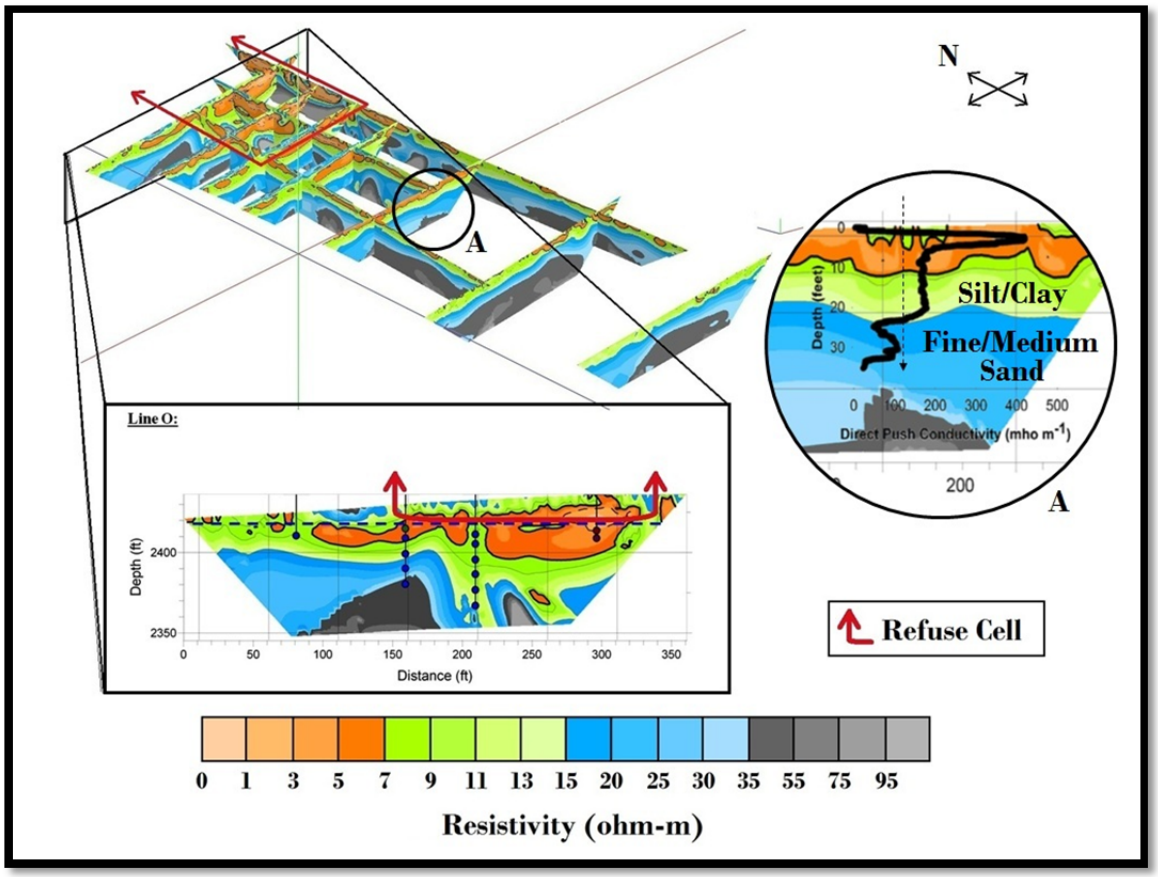

Figure 2.1. Composite ERI diagram of the former landfill in Cozad, NE. Figure represents results from 10 of the 19 ERI images obtained. Colored circles in cropped image (Line O) indicates locations and depths from which groundwater samples were obtained and provides an example of how samples were taken from different ERI-identified layers. Results of direct push Electrical Conductivity logging overlain on Line I in the TCE plume (A).

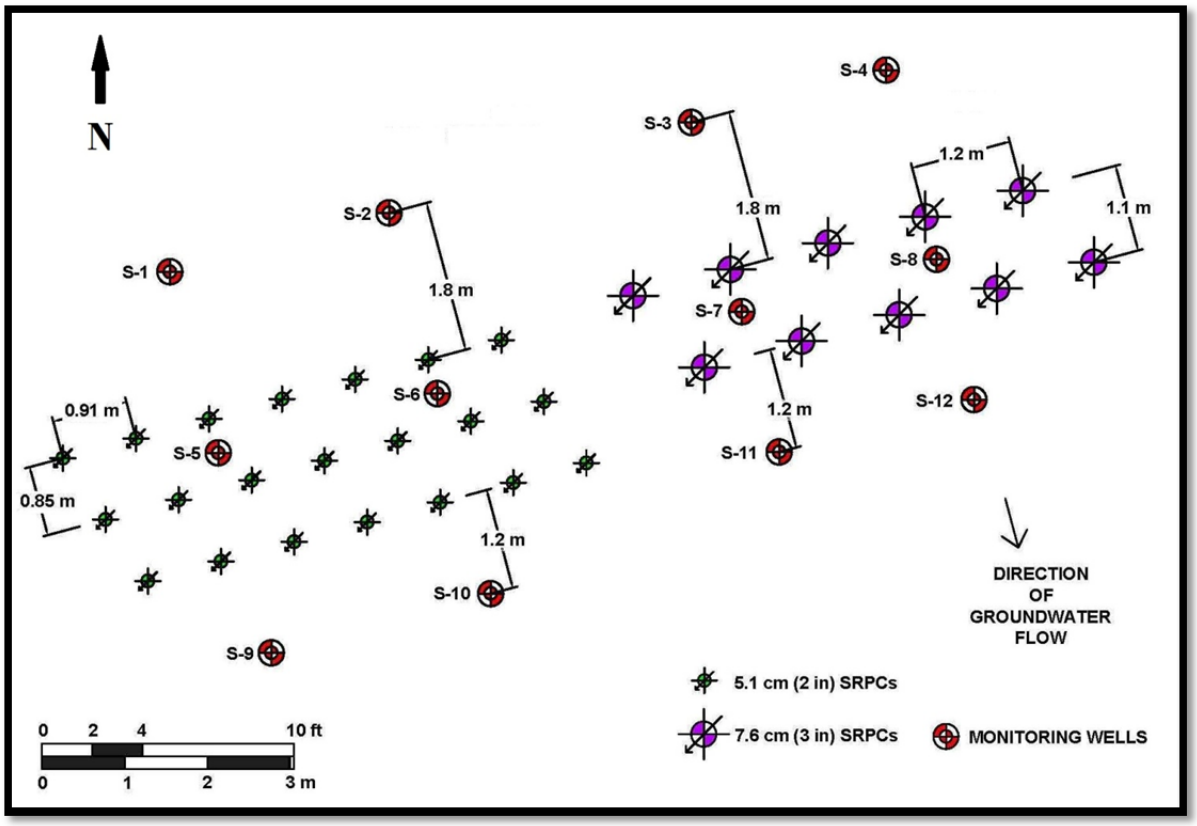

Figure 2.2. Field plot of the permeable reactive barrier of SRPCs and monitoring wells.

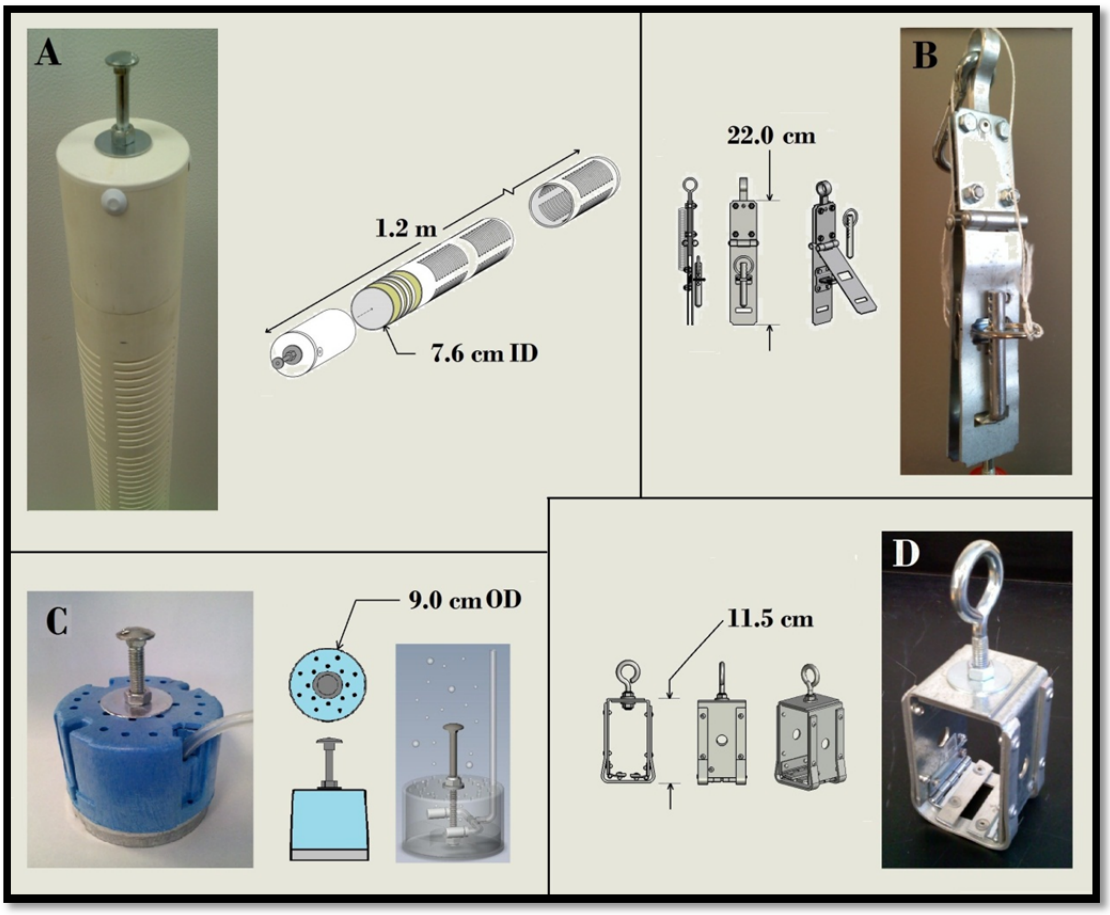

Figure 2.3. Photographs and schematics of field hardware used at field site: (A) 7.6-cm SRPC In Situ Candle Carrier (ISCC); (B) Candle Insertion Tool (CIT); (C) Pneumatic Recirculator; (D) Candle Removal Tool (CRT).

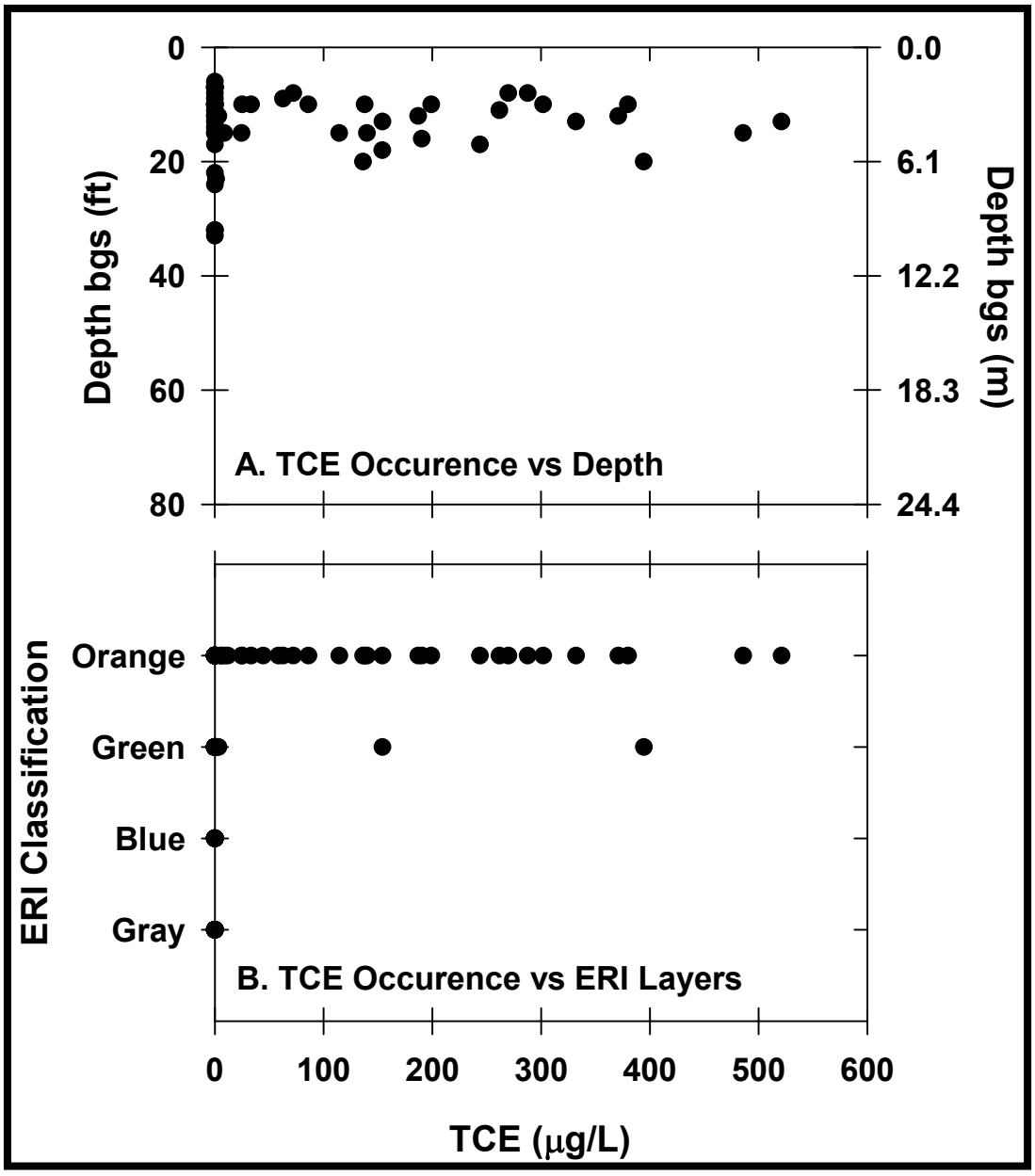

Figure 2.4. TCE occurrence in groundwater samples as a function of depth (A) and ERI layer (B).

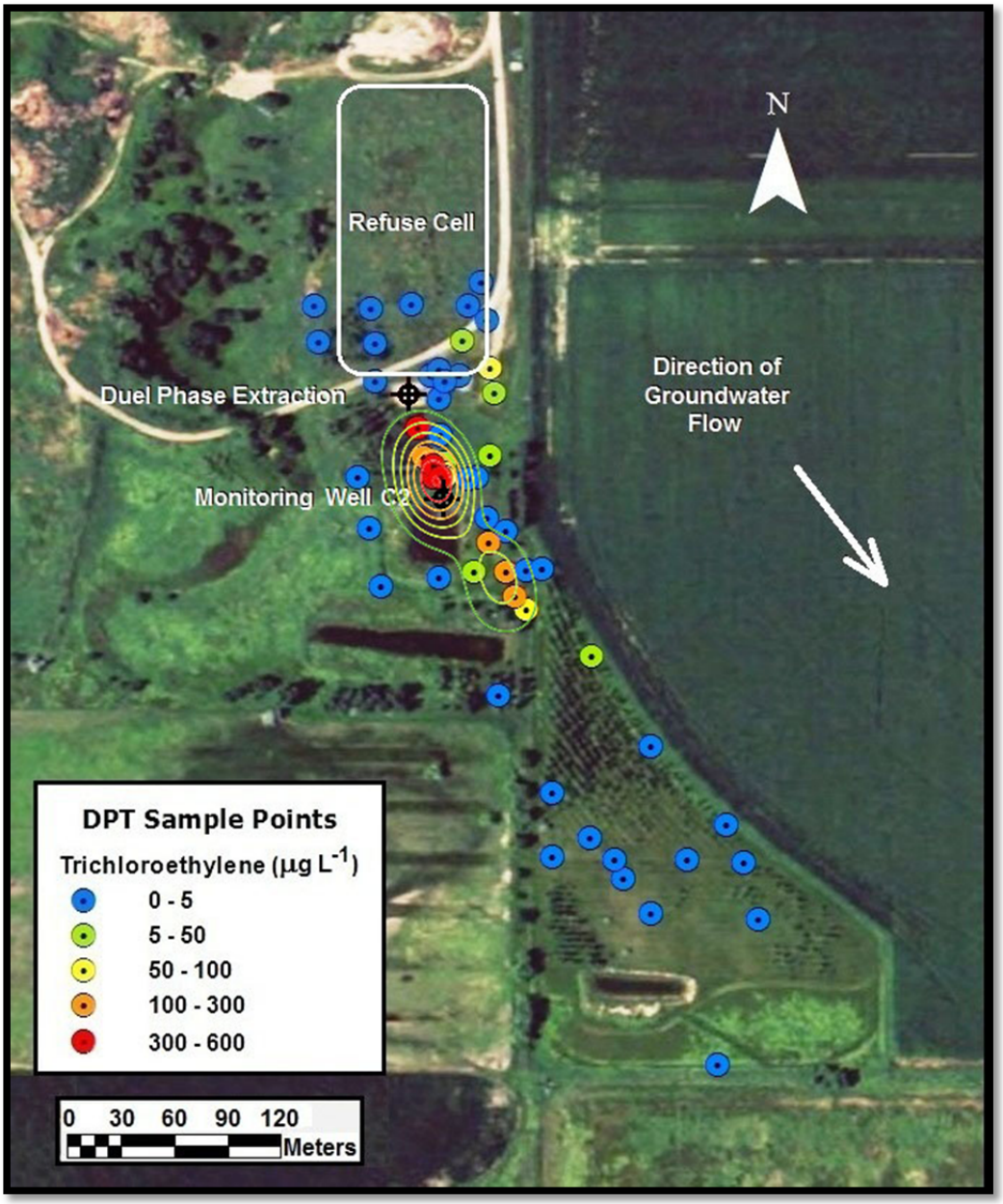

Figure 2.5. Aerial photo of Cozad landfill with TCE plume, and groundwater sampling locations superimposed.

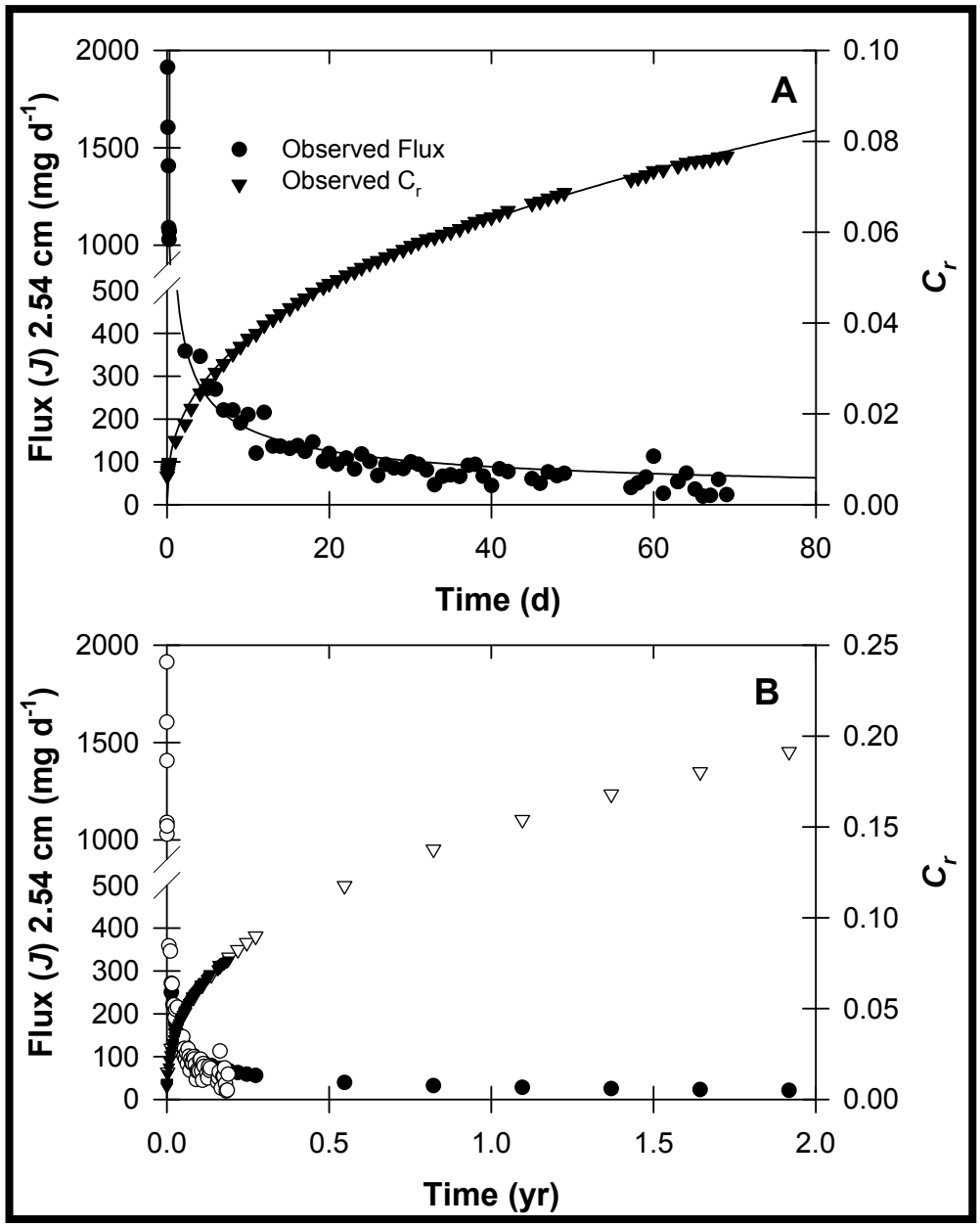

Figure 2.6. (A) Observed flux (*J*, mg d^{-1}) and C_r from 1.27-cm length SRPCs (5.1- cm diam) in water. (B) Observed *J* and C_r with projected values out to two years.

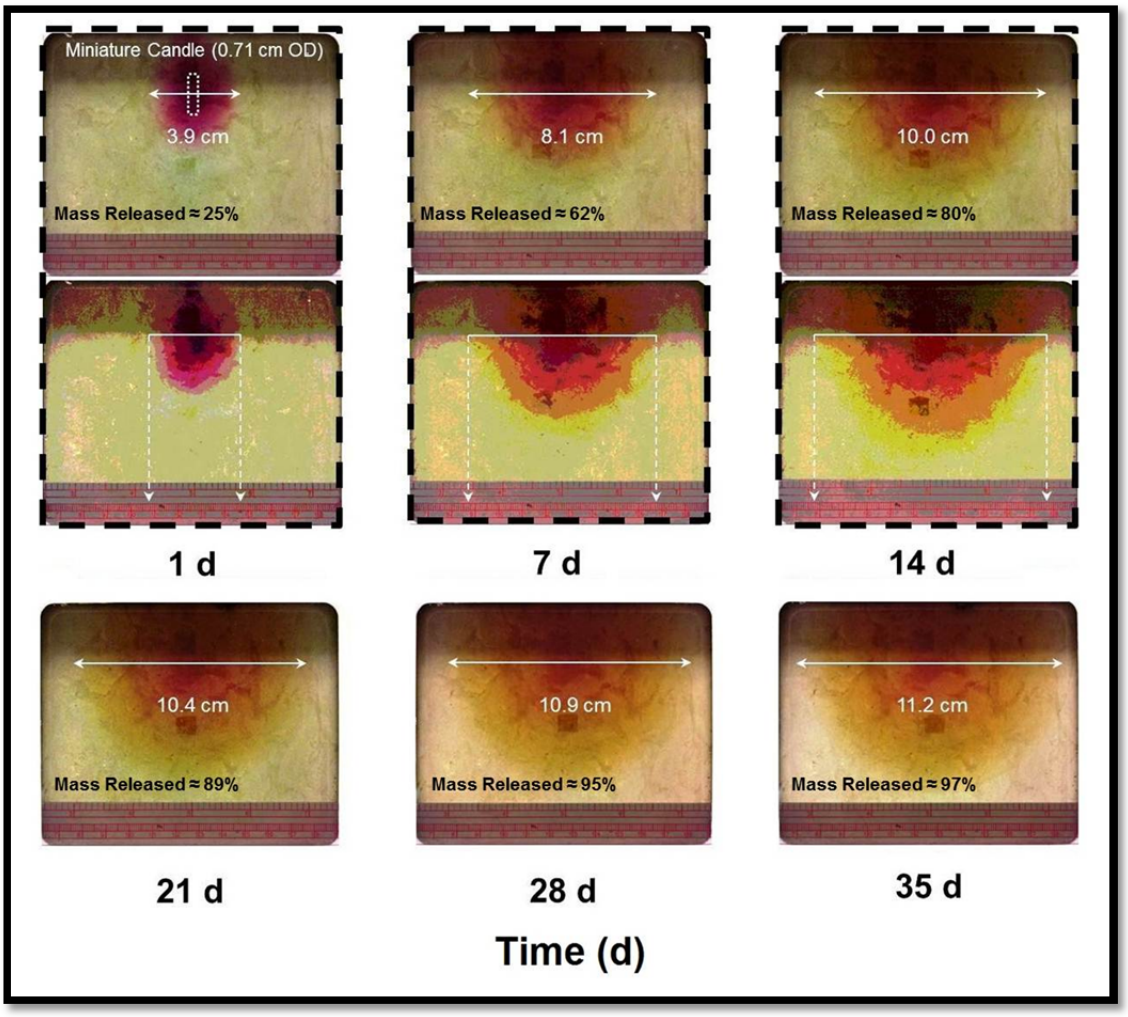

Figure 2.7. Temporal changes in diffusion distances (radius of influence) from miniature candles when placed in water-saturated, static, 2D tank packed with low permeable aquifer material (i.e., orange ERI region). Estimates of mass released were obtained from parallel experiments conducted in H_2O. Photos with dashed outlines show original photo (top) and digitally enhanced photo (bottom).

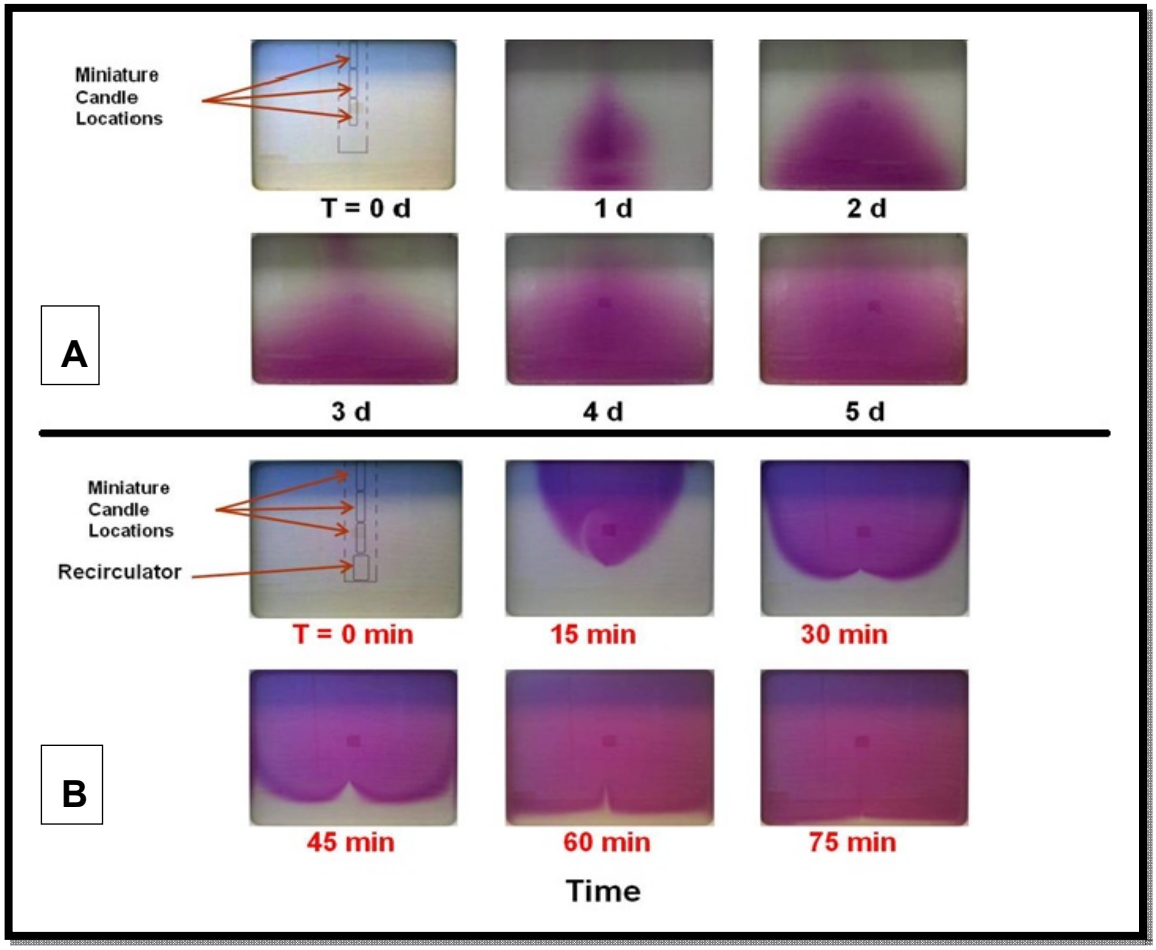

Figure 2.8. Temporal changes in permanganate diffusion patterns from three miniature candles placed in water-saturated, static, 2D tank packed with sand, with and without a pneumatic recirculator (B and A).

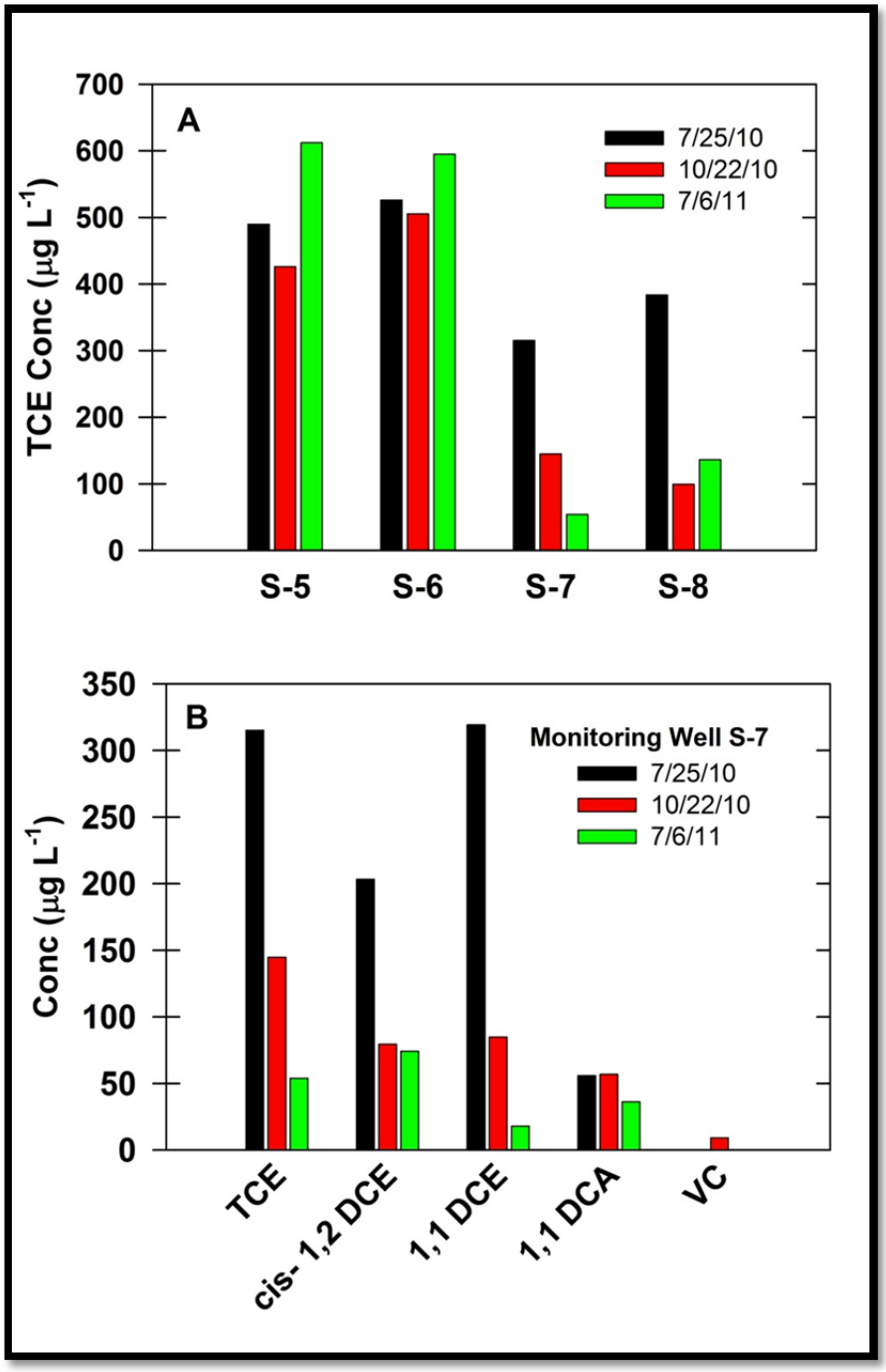

Figure 2.9. (A) Changes in mean TCE concentrations in monitoring wells embedded in SRPC treatment zone (S5-S8) before SRPC installation and 85 d and 342 d after (10/22/10 and 7/6/11) SRPC installation. Similar TCE fluctuations as in wells S5 and S6 have been historically observed at the site. (B) Changes in mean TCE and degradation products in monitoring well S-7.

Appendix A: Supplementary material

SM 2. Methods

SM 2.1 Direct push electrical conductivity logging

Direct Push Electrical Conductivity Logging (DPT EC) was conducted near monitoring well C2 and on line L (Fig. A1), 47 meters down-gradient (south-southeast) from C2. A Geoprobe® Direct Imaging Electrical Conductivity Probe was pushed to a depth of 10.7 m (35 feet) bgs through the two uppermost ERI layers described in the results section. Depth specific electrical conductivity and probe speed were collected on a Geoprobe® FC5000 Data Acquisition System. Services and equipment were provided by the University of Nebraska Conservation and Survey Division (CSD).

SM 2.2 Soil texture

Analyses of soil texture were performed on soil cores collected near monitoring well C2. Cores were sub-sampled at depths of 1.5, 3, 4.5, 6, 7.5 m (5, 10, 15, 20, and 25 feet). Samples were analyzed for bulk density and porosity (Soil Science Society of America, 1986). Additionally, soil texture was determined from sub-samples collected from the same locations stated above (Kettler et al., 2001).

SM 2.3 Soil oxidant demand

We determined soil oxidant demand from the same soil cores used for soil texture analyses. Procedures used are described in ASTM D7262-07. Sub-samples were extracted from depths of 1.5, 3, 4.5, and 6 m (5, 10, 15, and 20 feet). Sample aliquots were centrifuged in a Sorvall® T6000B laboratory centrifuge to remove MnO_2 and suspended sediment. Aliquots were then

diluted if necessary and analyzed at 525 nm on a Hach® DR 2800 Spectrophotometer standardized using Method 4500-$KMnO_4$ (APHA et al., 2005).

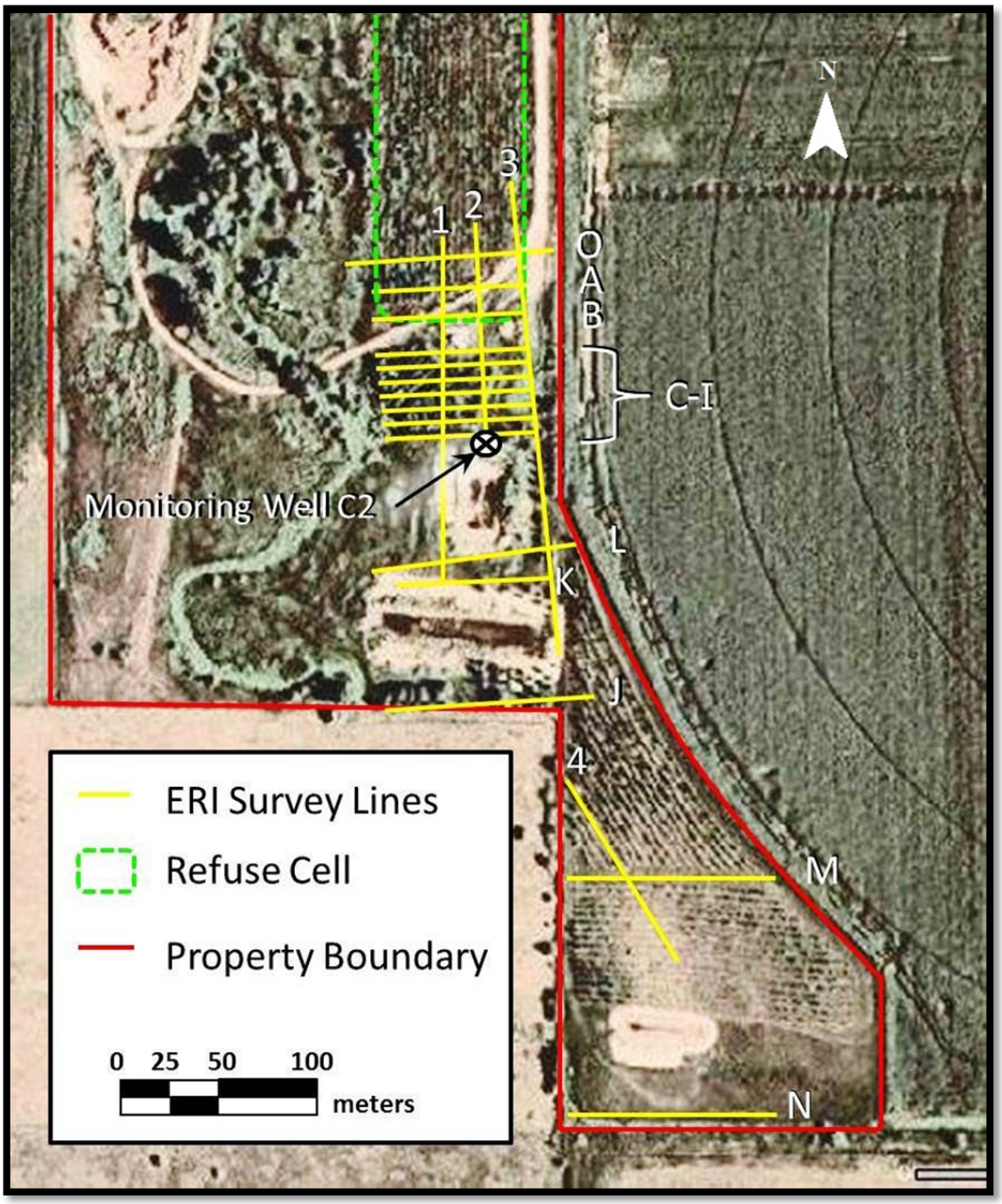

Figure A1. Aerial photo of Cozad Landfill with locations of ERI lines. Six ERI lines (O, A, B, 1, 2, and 3) acquired images that overlapped the refuse cell, the remaining lines were down gradient from the refuse cell. Lines labeled 1 and 3 consist of multiple 110 meter lines overlapping by 55 meters. Overlapping ensured a continuous image across the entire length of the survey line.

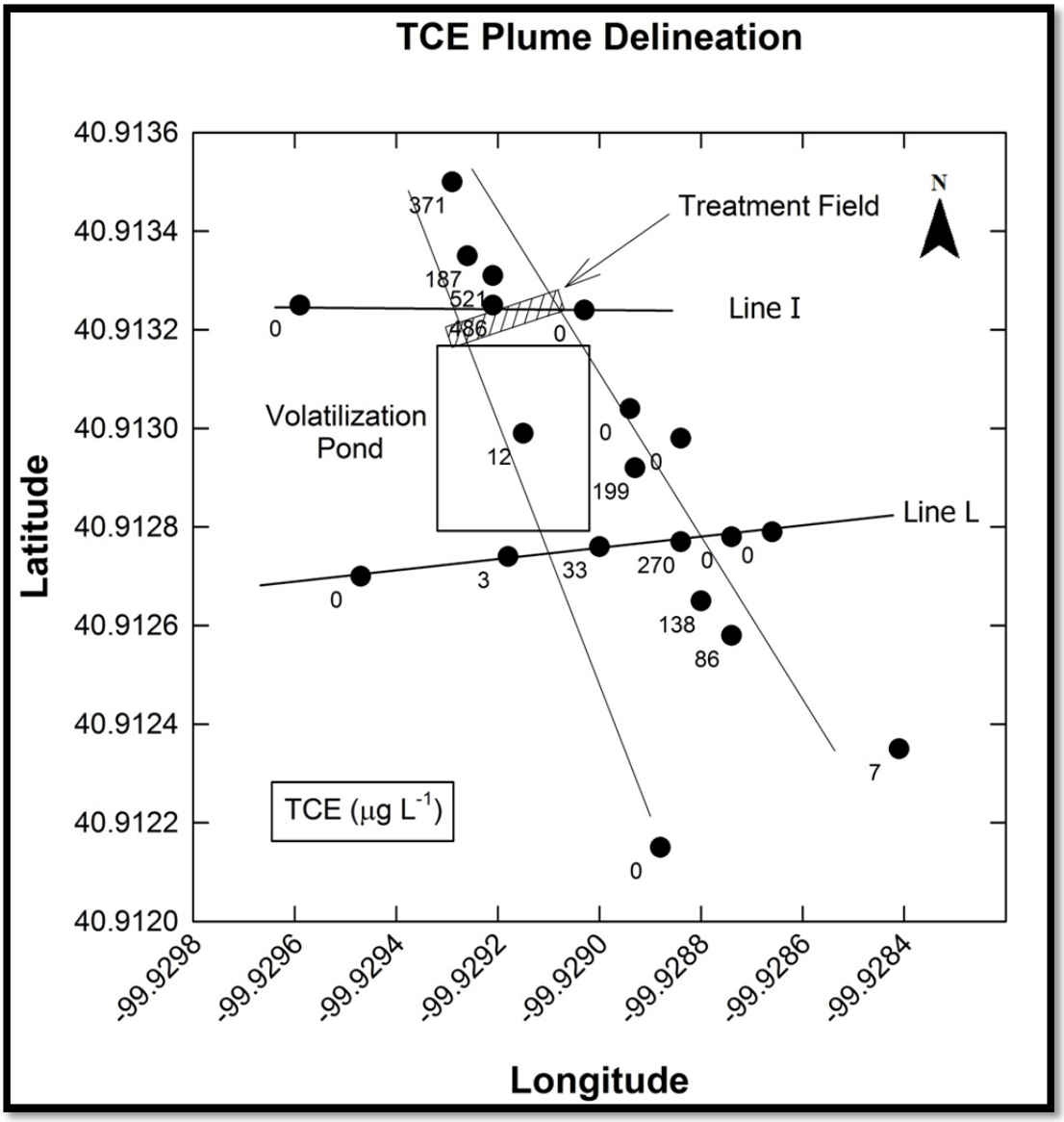

Figure A2. Location of treatment field containing 5.1 and 7.6-cm diam SRPCs in relation to TCE concentrations (μg L^{-1}) determined via direct push sampling and ERI lines (Fig. A1).

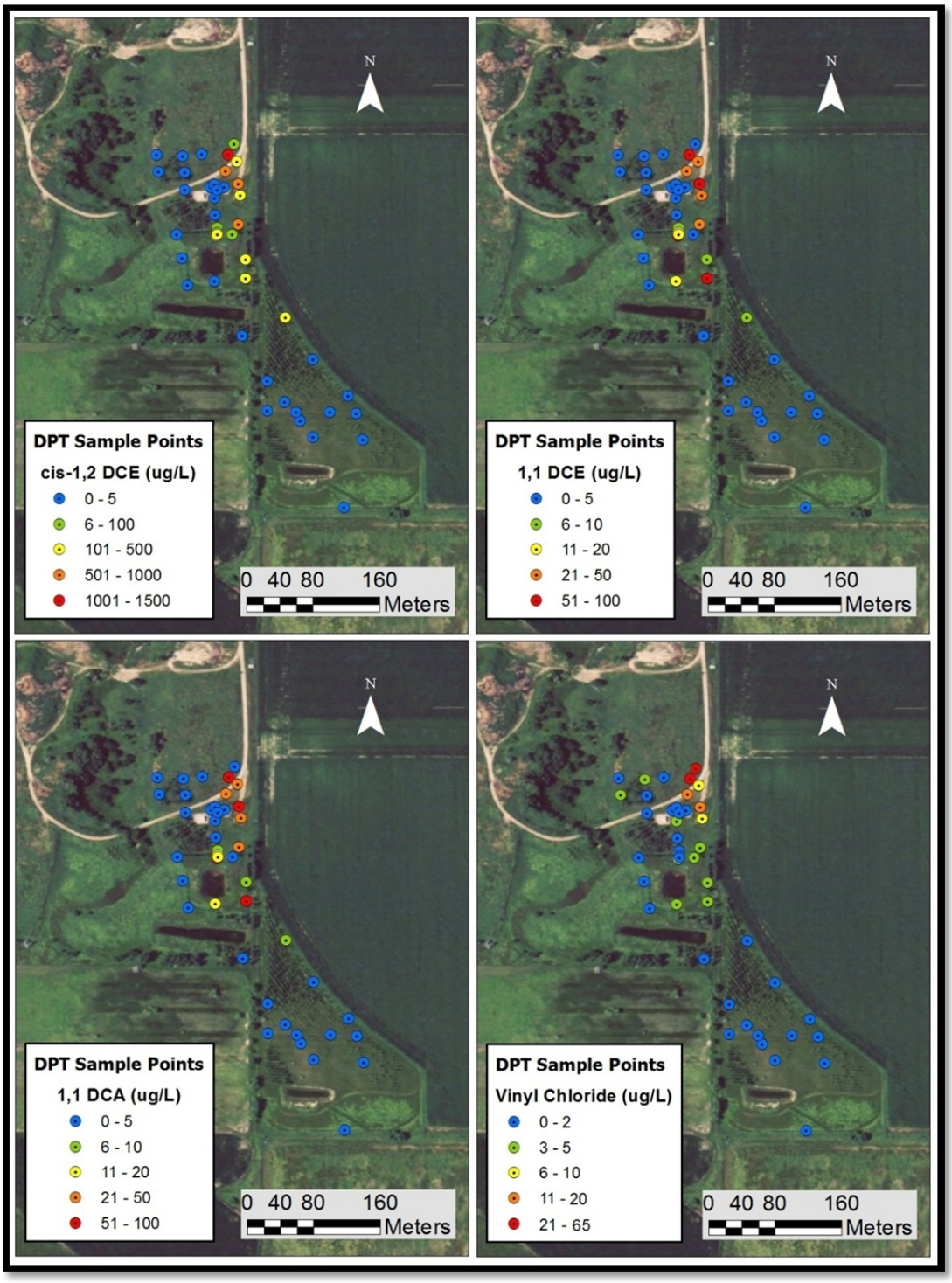

Figure A3. Aerial view of Cozad landfill with the highest degradation product concentration collected from each sample location.

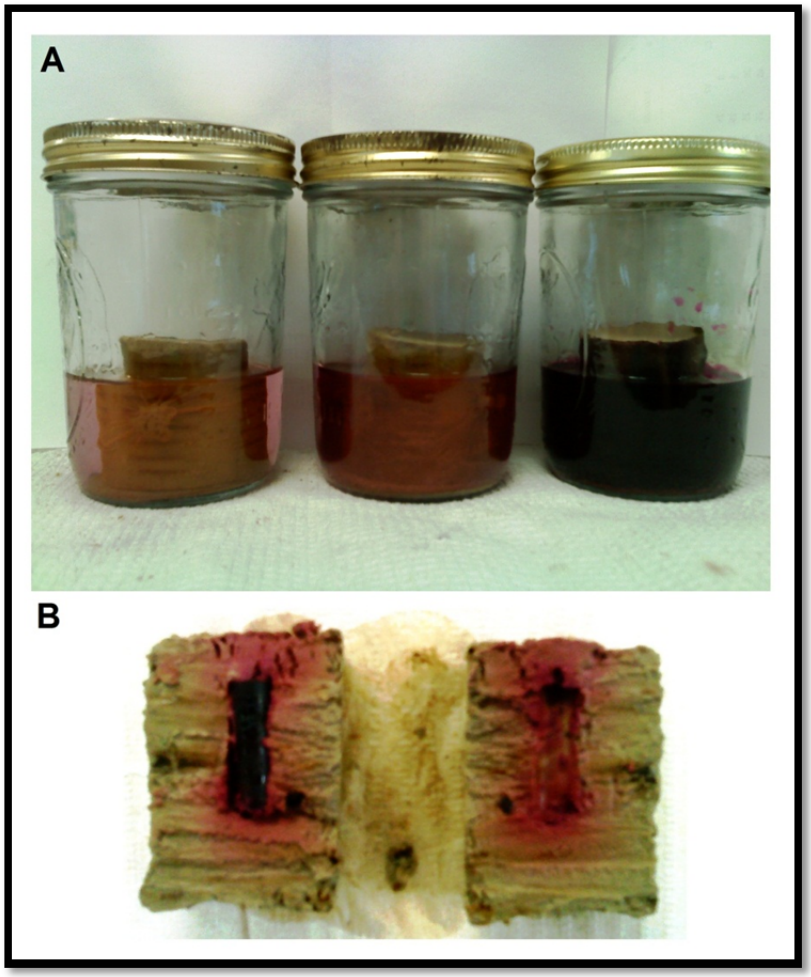

Figure A4. Photographs of permanganate diffusion experiments (top) where intact soil cores (4.25 cm diam) from low permeable aquifer (orange ERI region) was embedded with a mini-SRPC and saturated in H_2O under static conditions. (Bottom) Permanganate diffusion from mini-SRPC after 24 h.

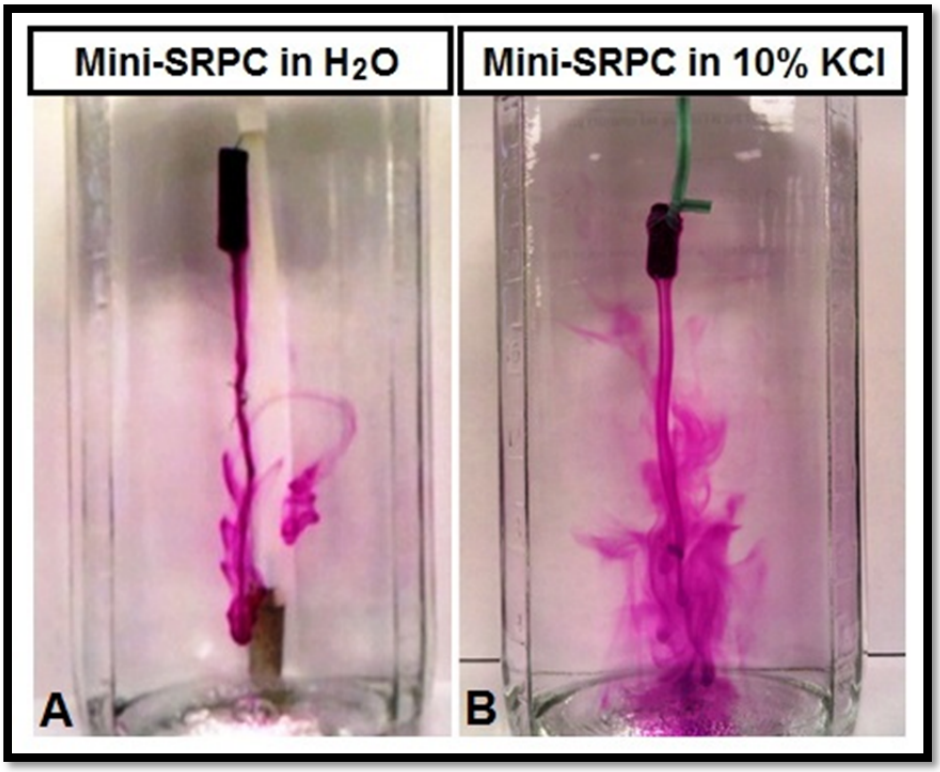

Figure A5. Streams of permanganate flowing downward from mini-SRPC in (A) water and (B) 10% (w/v) KCl.

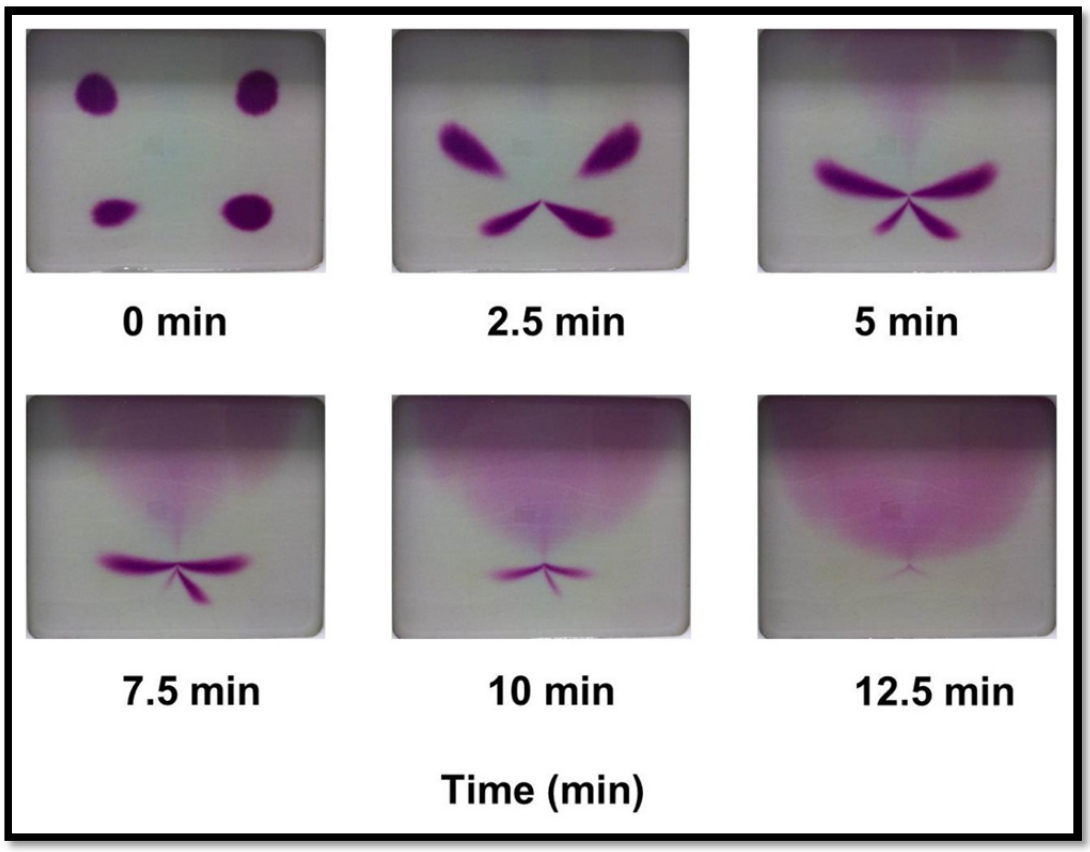

Figure A6. A 12.5-min time sequence of photographs showing permanganate movement when in the presence of a pneumatic recirculator. Experimental setup was identical to results provided in Fig. 2.8.

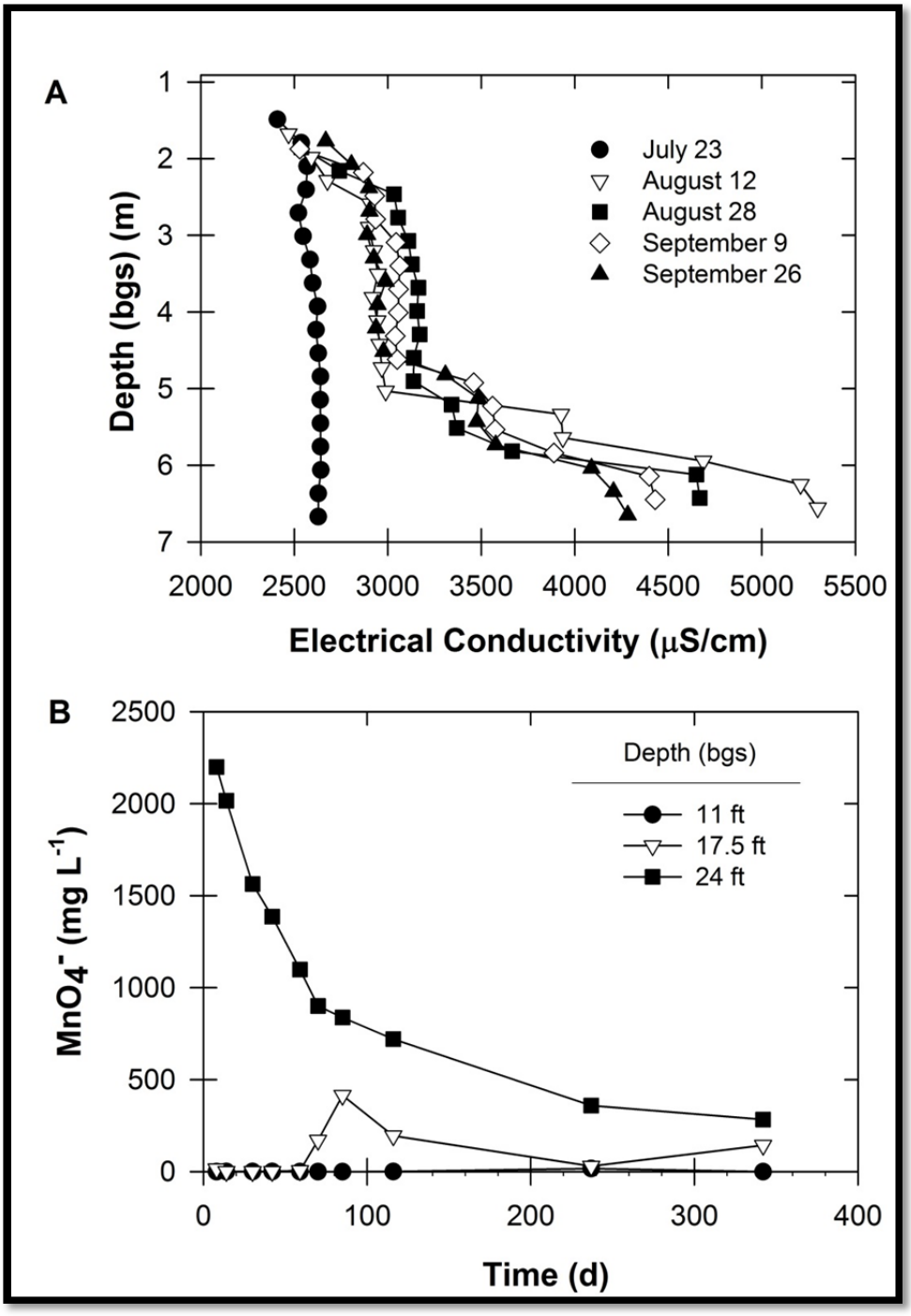

Figure A7. Effects of density driven flow on permanganate distribution within the PRB prior to pneumatic recirculator installation. Recirculators were installed on 7/14/11. A) Conductivity profile of monitoring well S-7. B) Permanganate concentrations with depth in monitoring well S-7.

References

American Public Health Association (APHA), American Water Works Association (AWWA), Water Environment Federation (WEF), 2005. Standard Methods for the Examination of Water & Wastewater; Method 4500 KMnO4. Port City Press, Baltimore, MD.

ASTM Standard, 2007. Standard test method for estimating the permanganate natural oxidant demand of soil and aquifer solids (Method D72262-07). West Conshohocken, Pennsylvania: ASTM International. http://www.astm.org.

Kettler, T., Doran, J., Gilbert, T., 2001. Simplified method for soil particle-size determination to accompany soil quality analyses. Soil Science Society of America Journal 65, 849-852.

Soil Science Society of America, 1986. Methods of Soil Analysis, Part 1: Physical and Mineralogical Methods. Madison, WI: American Society of Agronomy, Inc; Soil Science Society of America, Inc.

Appendix B: Slow-release permanganate candle making procedure

CAUTION:

- **Wear apron or lab coat and gloves at all times when handling $KMnO_4$ and hot wax!**
- **Wear safety glasses or face shield at all times when mixing hot wax!**
- **Wear facemask and/or work in fume hood when handling $KMnO_4$ crystals to prevent inhalation of $KMnO_4$ dust!**
- **Minimize combustibles in immediate area surrounding production!**
- **Containers placed in drying oven may be hot to the touch, use caution when handling!**
- **Keep a 5-gallon metal pail of water available to rapidly extinguish permanganate and wax mixture if smoking/burning occurs!**

1. Melt approximately 7-10 pieces of Paraffin Wax (5 cm x 5 cm x 5 cm) on high (65±5°C) in a commercial wax melter.
2. As wax melts transfer it to a ceramic slow cooker set on high (maximum observed temperature after 2.75 hr without use: 95°C; maximum observed temperature during use/production: 74°C) to maintain sufficient wax reserves. Repeat step one as necessary.
3. Preheat 600 g $KMnO_4$ in a drying oven set to 90±5°C for 10 to 20 min.
4. Place melting pot on a hot plate preheated to 95°C.
5. Add approximately 350 mL of melted paraffin wax to the melting pot.
6. Insert mixing rod and propeller into the wax then start on medium speed to prevent wax from splattering.
7. Pour approximately 600 g of $KMnO_4$ into the melted wax until a slurry of wax and $KMnO_4$ the consistency of a thin milk shake is attained. Move the pot around to ensure the solution is well mixed.
8. If congealing prevents fluid mixing place melting pot into drying oven for several minutes to aid in re-melting the mixture, then continue mixing.
9. If necessary add additional $KMnO_4$ slowly until the shiny wax layer at the surface disappears and the mixture's consistency is that of a thick milk shake. Poor into cardboard molds to the top.
10. Tamp molds gently to remove any entrapped air from the mixture.
11. Allow candle to cool upright at room temperature (12-24 hr).

Appendix C: Evaluation of volatilization pond performance

Objective: The City of Cozad installed three ponds at the former landfill in an attempt to induce volatilization. While viewed as a low-cost, low-technical approach, the effectiveness of these ponds had not been studied. Our objective was to determine if VOCs were entering the ponds and becoming volatilized. Each pond was approximately 2 m deep from the water surface to the bottom and varied in surface area (1,200 m^2 for North pond). The installation of the volatilization ponds began in 1998 and the last expansion of the North pond was completed in 2010.

Procedure: To evaluate pond performance ground and surface water was collected in and surrounding the North pond for VOC analysis. Water samples from inside the pond were collected using a Van Dorn bottle at a depth of 0.3 m along a transect running through the center of the pond from the North edge to the South edge. Additionally, a sample was collected 0.3 m from the bottom in the center of the pond. Ground water samples were collected via direct push sampling along each edge of the pond.

Results: Water samples from the pond collected at the 0.3 m depth had no detectable VOCs. However, the sample collected at the bottom of the pond had 12 μg L^{-1} TCE. The highest concentrations of TCE from the direct push samples were along the north edge near the centerline of the pond (332 μg L^{-1}) and at the southeast corner of the pond (270 μg L^{-1}). TCE was also detected below the

MCL along the south and east edges of the pond. These results indicate that volatilization is effectively reducing the mass of TCE inside the ponds. However, the ponds may not be deep enough to intercept the vertical extent of the plume.

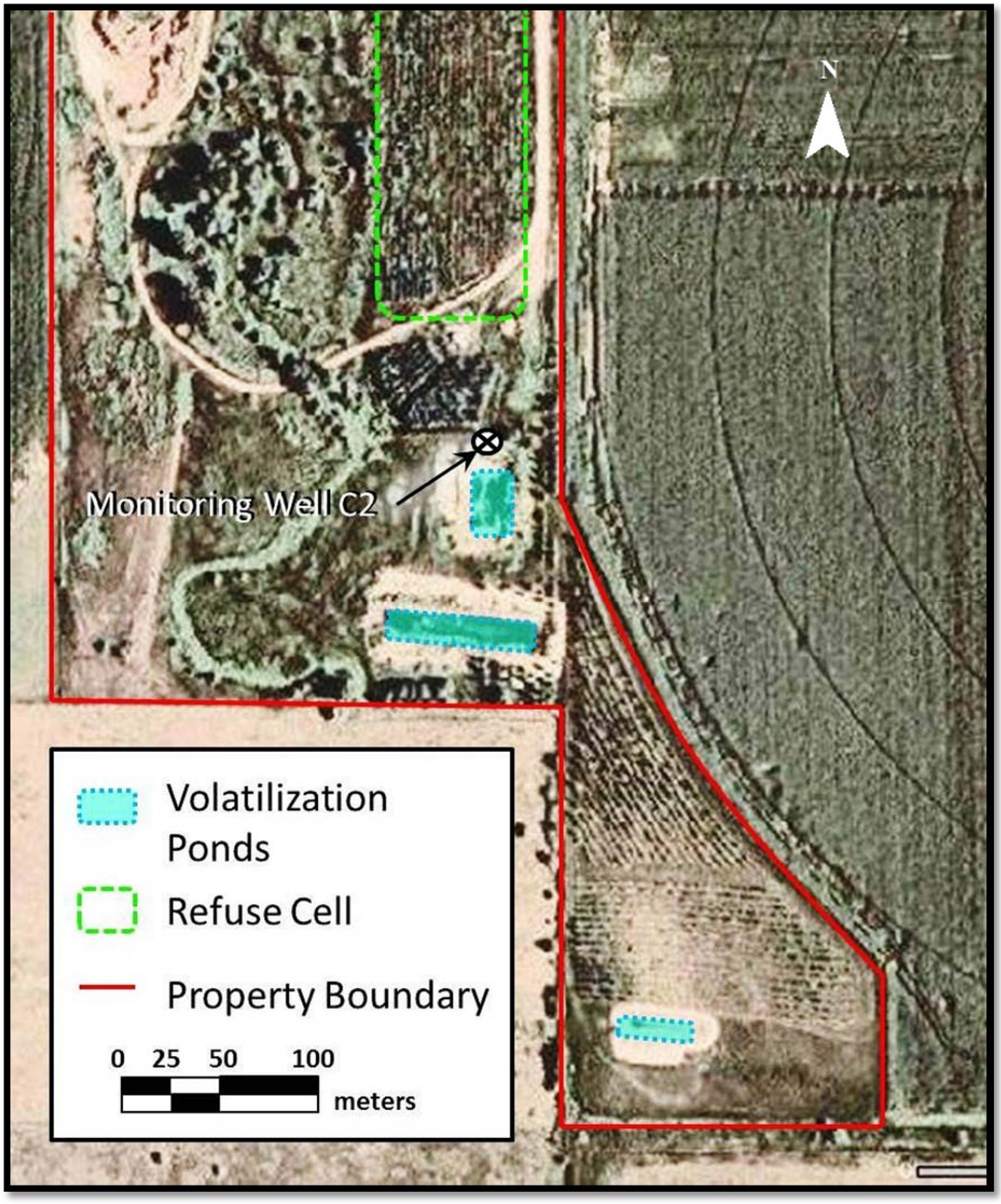

Figure C1. Aerial photo of the former Cozad landfill with locations of volatilization ponds overlain. Surface water samples were taken inside the north pond near monitoring well C2. Direct push groundwater samples were taken surrounding the north pond. Results of sampling are reported in Figure C2.

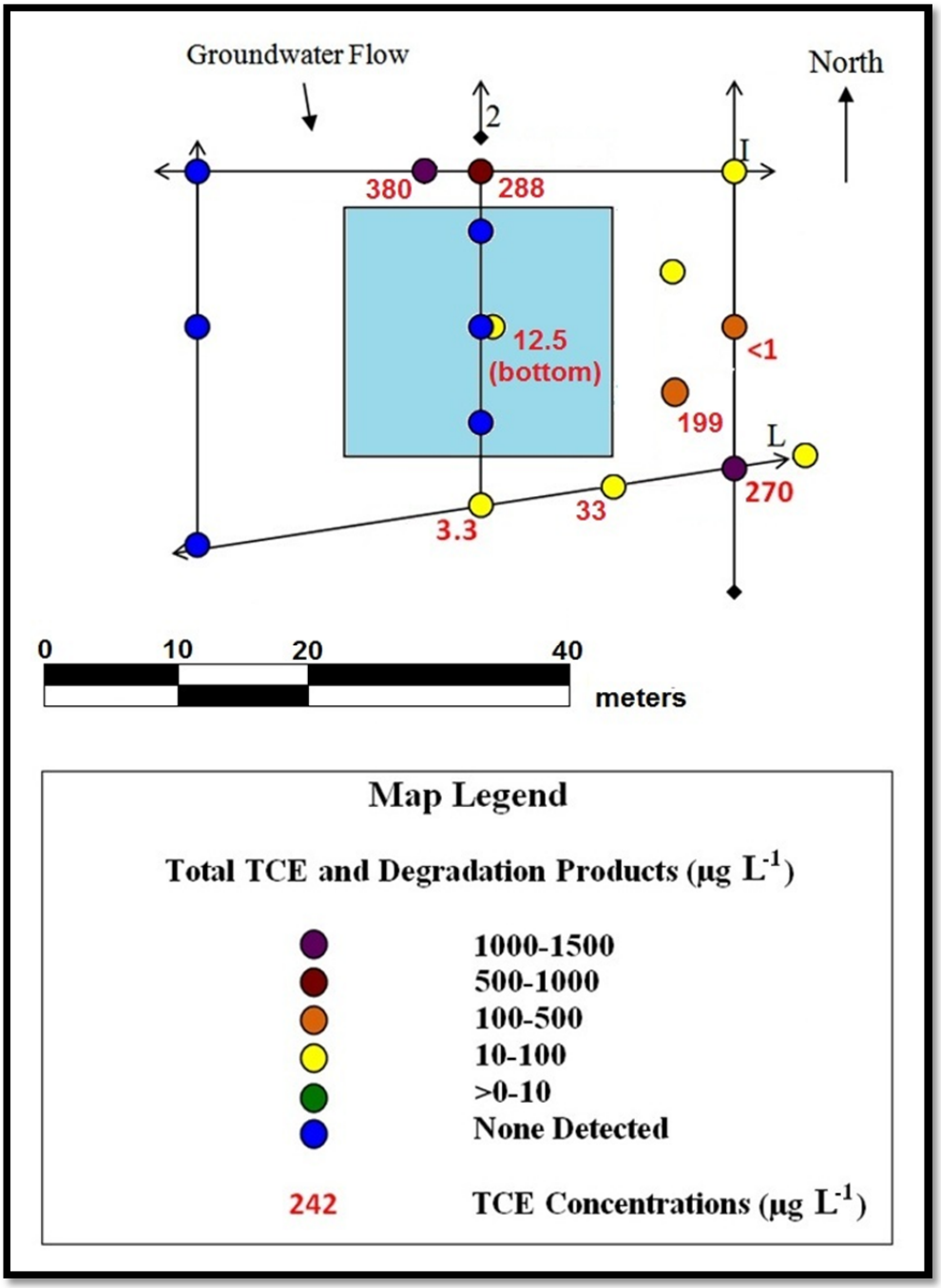

Figure C2. Results of ground water and surface water VOC sampling in and around the north volatilization pond at the former Cozad landfill. Near surface samples from the pond had no detectable VOCs, but VOCs were detected above MCLs at the bottom center of the pond. Circles represent sample points. Color of circles represents total TCE and degradation product concentration. TCE concentrations are in red.

Appendix D: Polymeric phosphate amendments to SRPCs

Objective: Recent research has identified the effective use of sodium hexametaphosphate (SHMP) as a stabilization aid to prevent MnO_2 pore clogging during in situ chemical oxidation with permanganate. We manufactured mini-SRPCs with an amendment of tetrapotassium pyrophosphate (TKPP, $K_4P_2O_7$), a polymeric phosphate similar to SHMP. Our objective was evaluate the permanganate release characteristics in the presence of the TKPP.

Procedure: Mini-SRPCs were manufactured with a chemical composition of potassium permanganate, TKPP, and paraffin wax mixed at a 3:2:2 ratio (w/w/w). The mini-SRPCs were placed in deionized water and subsampled at various times over the course of 55 d. Samples were analyzed for MnO_4^- concentration and data was evaluated to determine permanganate flux and concentration ratio.

Results: When compared with non-TKPP containing mini-SRPCs (Chapter 2, Sec 2.3 & 3.3), the TKPP-SRPC flux decreased to an asymptote that created a much more linear plot of *Cr*. This is a highly favorable behavior for a long term controlled release system. Further investigations should include characterization of: 1) TKPP release performance, 2) TKPP MnO_2 stabilization in the presence of contaminated solvent, and 3) TKPP-SRPC performance in porous media, flowing water, and contaminants are warranted.

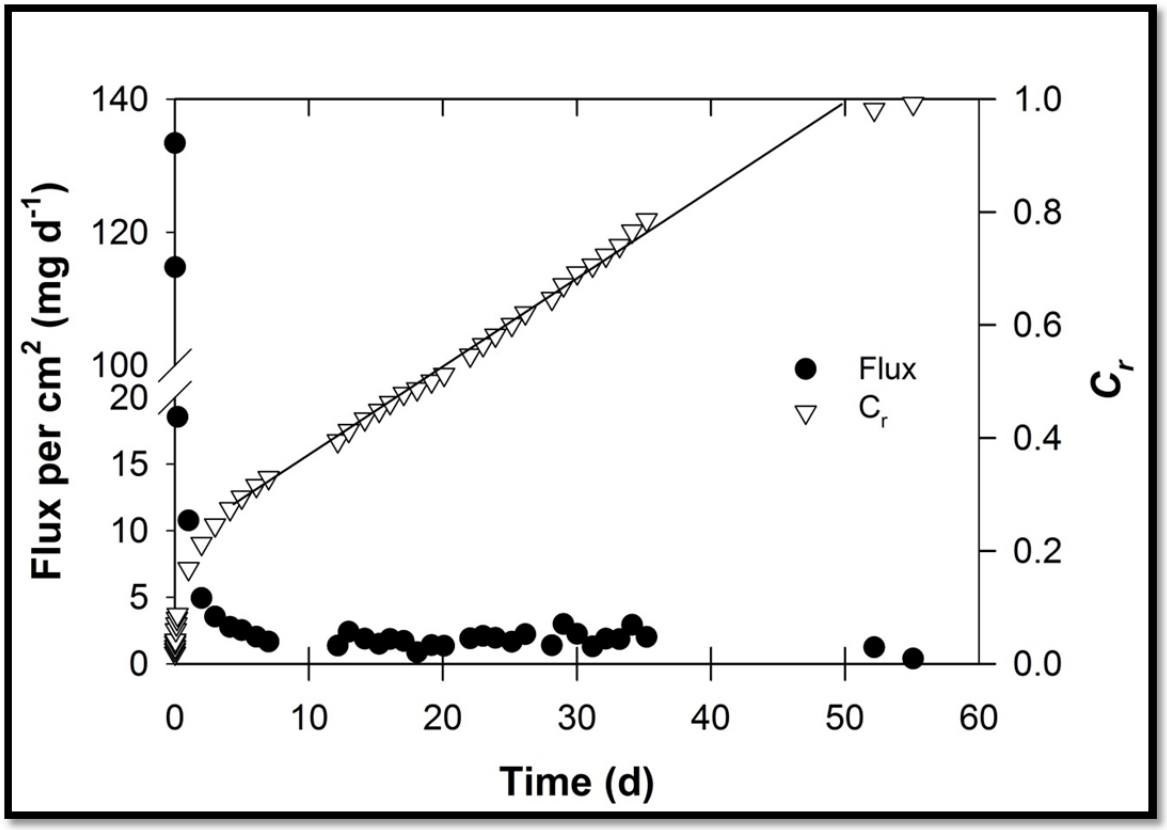

Figure D1. Flux and concentration ratio (C_r) of a 3:2:2 (w/w/w) $KMnO_4$: TKPP : Paraffin mini-SRPC.

Appendix E: Design and prototype of reinforced hollow DPT SRPCs

Objective: Concerns that void space between the direct push borehole wall and the surface of inserted SRPCs could facilitate density driven sinking of permanganate prompted investigation into new designs. The objective of the new design was to eliminate or minimize the borehole to SRPC gap.

Procedure: A single layer of 1.25 cm x 1.25 cm (grid size) #19 galvanized mesh wire cloth was inserted against the inside wall of a 7.6 cm (ID) cardboard tube. A 3.2 cm (ID) PVC tube was attached to the center of a 7.6 cm poly plug and inserted into the wire mesh and cardboard assembly. A molten 4.6:1 (w/w) permanganate/paraffin wax slurry was poured inside of the cardboard assembly around the PVC tube and allowed to cool.

Results: The new SRPC design should exhibit considerable improvements in strength over the non-reinforced SRPCs. If additional strength is still required fiberglass reinforcement may also be utilized. The inner PVC tubing can be attached to an expendable tip and push rods can push the tip into the ground, thus, pulling the reinforced SRPC with it. The SRPC and expendable tip can be manufactured to the same outside diameter, therefore, creating minimal gap space between the borehole and the surface of the SRPC. Additionally, a 7.6 cm reinforced hollow SRPC creates a smaller borehole and has a greater mass of permanganate than the 5.1 cm DPT SRPCs used in the field study.

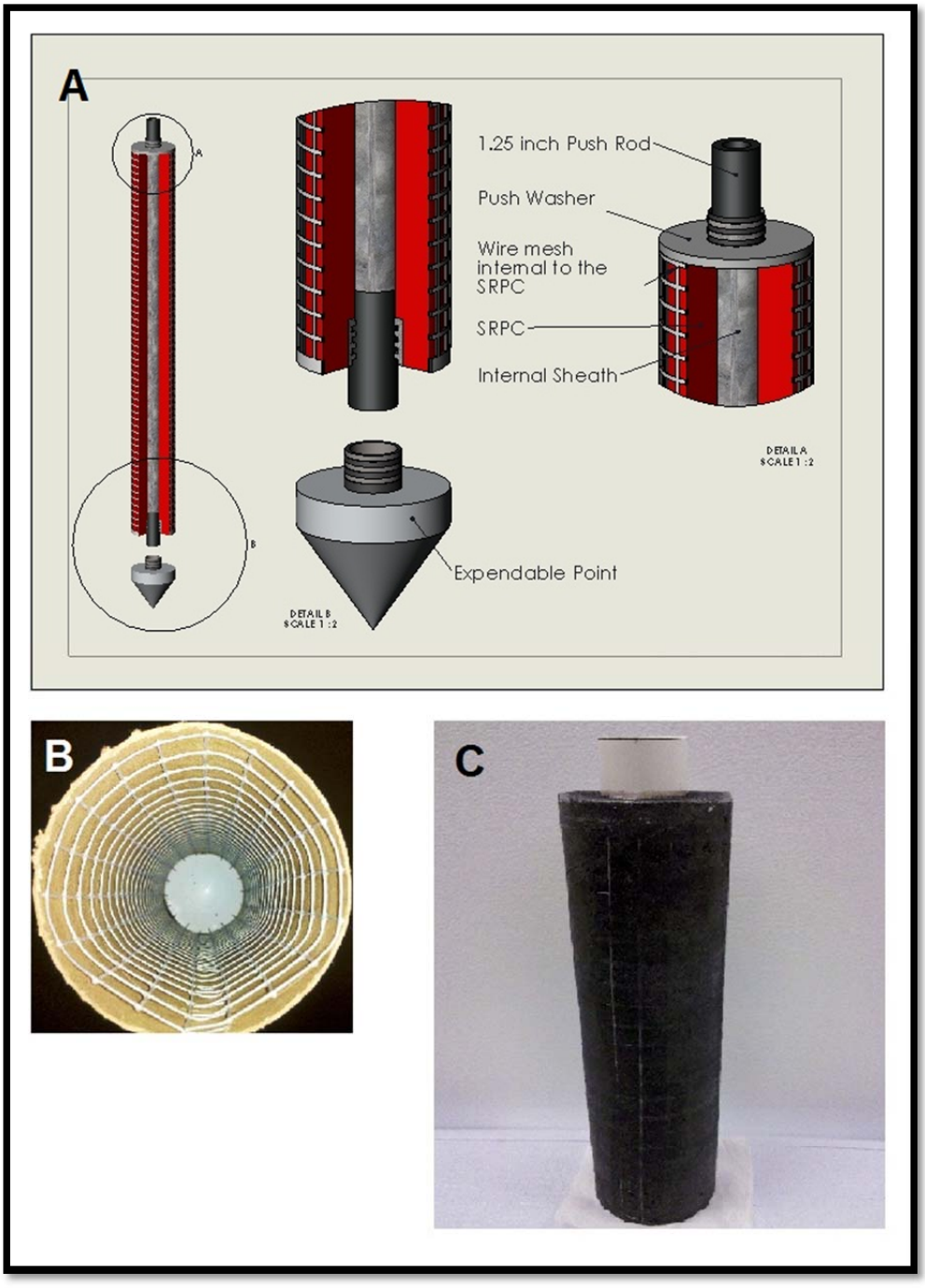

Figure E1. A) diagram of reinforced hollow SRPC design and tooling, B) wire mesh fabric placed inside of 7.6 cm (ID) cardboard mold, C) prototype of a reinforced hollow SRPC.

Appendix F: Evaluation of recirculator in heterogeneous media

Objective: Mini-SRPCs with and without a recirculator were tested in heterogeneous media to determine if density driven sinking of permanganate from SRPCs would prevent effective distribution of permanganate into a lower permeable zone between two higher permeable layers.

Procedure: A 12.7 cm (ID) column 38 cm in length sealed on the bottom was filled with 10.8 cm of medium sand followed by 15.2 cm of fine sand and 7.6 cm of medium sand then filled with deionized water. A 1.3 cm (ID) well, screened 10 cm in the center of the fine sand, was inserted into the center of the column to the bottom of the fine sand. For the first experiment a string of three mini-SRPCs were inserted into the well and permanganate migration was observed. In a subsequent experiment the same column conditions were repeated, and a recirculator was inserted into the bottom well.

Results: During the experiment without the recirculator permanganate was first observed at the bottom of the column in the medium sand and slowly worked its way upward but failed to reach the top of the fine sand after 14 days. Conversely, during the experiment with a recirculator permanganate was first observed at the interface between the fine sand and upper medium sand in less than 1 hour. The permanganate front moved downward completely saturating the fine sand in less than 6 hours. At 6 hours

permanganate migrated less than 3 cm into the medium sands above and below the fine sand.

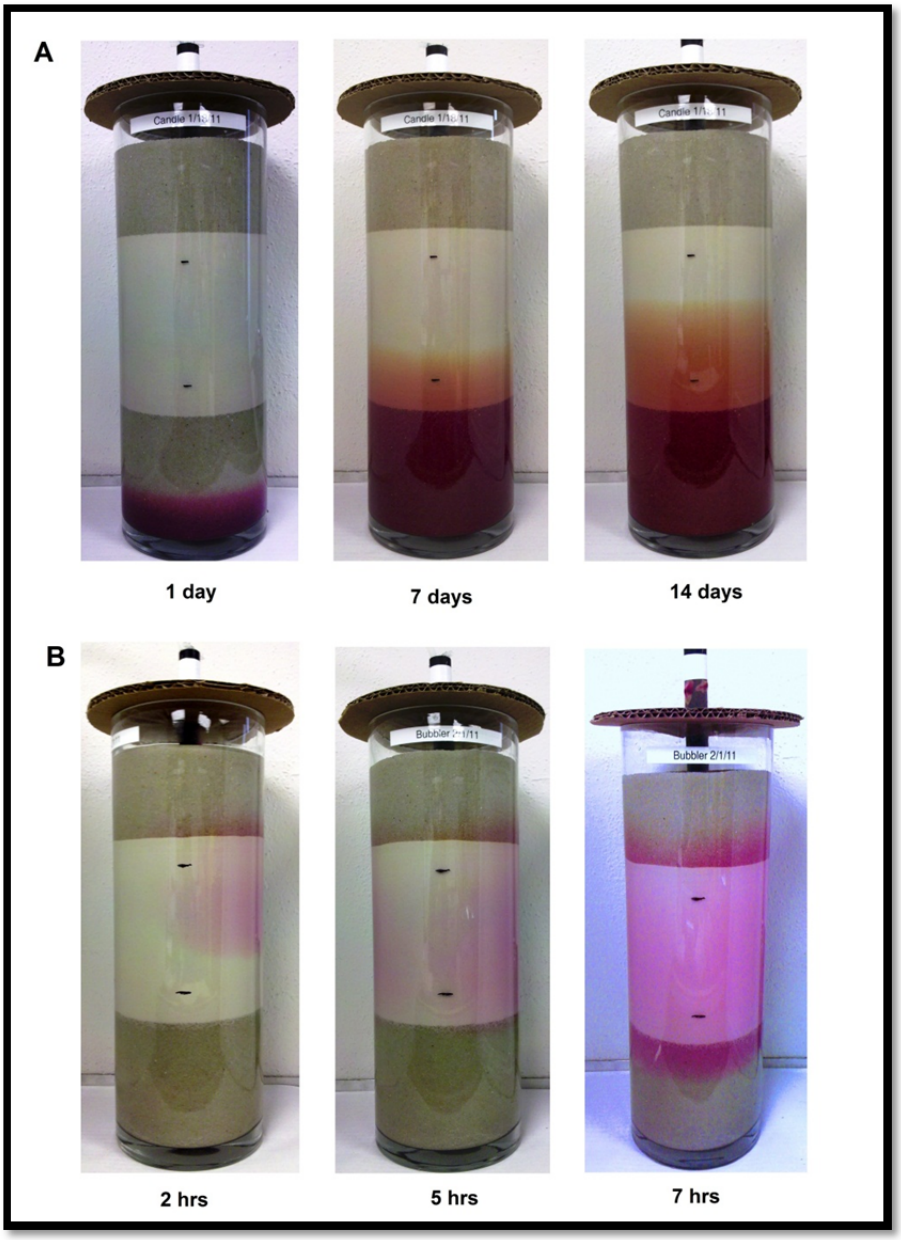

Figure F1. A) 4.6:1 SRPCs (x3) in a heterogeneous column without a recirculator at 1, 7, and 14 days. B) 4.6:1 SRPCs (x3) in a heterogeneous column with a recirculator at 2, 5, and 7 hours. Well is screened between black lines in the central fine sand region.

Appendix G: Evaluation of recirculator in low permeable media

Objective: A mini-SRPC with a recirculator was placed into low permeable media in a 2D tank to observe permanganate migration through the media. Of interest was the rate at which permanganate moved and the shape of the permanganate front.

Procedure: Saturated aquifer material (Silty-Clay) collected from aquifer cores was cut and packed into a 14 cm x 12.7 cm 2D tank. A section of low permeable media was cut out and replaced with a slotted well, sand filter pack, and bentonite seal. A recirculator and one mini-SRPC were placed into the bottom of the well and migration of permanganate was observed. Water in the tank was stagnate with the exception of movement from the recirculator.

Results: Permanganate was visible in the sand filter pack in less than 5 min. The filter pack was completely saturated with permanganate in 3 h. However, the diffusion rate of the permanganate front through the aquifer material was slower than that without the sand pack and recirculator in the direct push simulation described in Chapter 2. However, the vertical migration of the permanganate downward was less significant with a recirculator than without. This indicates that when recirculators are in use the rate of migration may be inhibited, but a greater percentage of permanganate will be transported through the treatment zone.

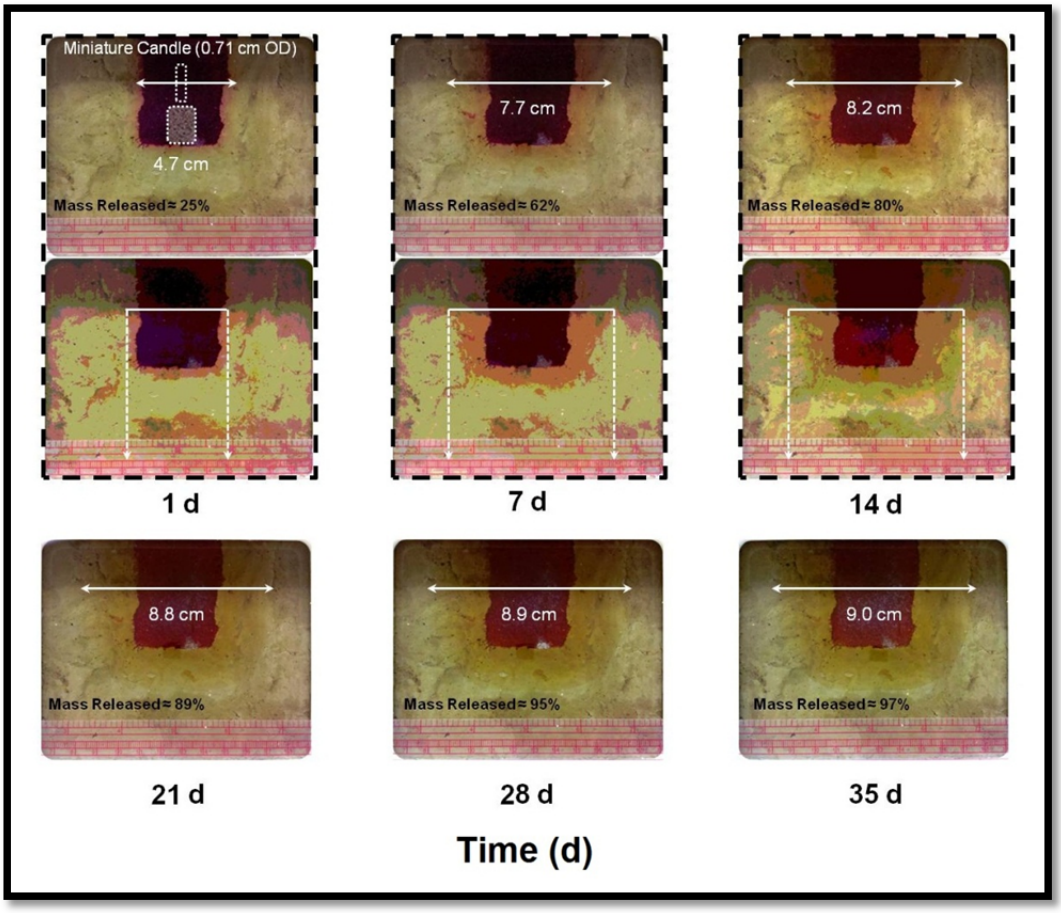

Figure G1. Temporal changes in diffusion distances (radius of influence) from miniature candles when placed in a simulated well in a water-saturated, static, 2D tank packed with low permeable aquifer material (i.e., orange ERI region). Estimates of mass released were obtained from parallel experiments conducted in H_2O. Photos with dashed outlines show original photo (top) and digitally enhanced photo (bottom).

Appendix H: Slow-release permanganate candle production and equipment supply lists

Table H1. In Situ Candle Carrier (ISCC) supply list.

Equipment/Tool	Manufacturer/Supplier	Model/SKU	Quantity	Price ($)[1]
3” ID x 3’ L Size: #120 Slotted PVC Casing with Threaded Cap	Titan Industries (Aurora, NE)	NA	1	35.00/ea
3/8” x 3” Carriage Bolt Zinc Plated	Crown Bolt, Inc (Home Depot)	030699055807	1	21.24/50
3/8” x 1 ½” Fender Washer Zinc Plated	Crown Bolt, Inc (Home Depot)	030699201204	2	20.37/100
3/8” -16 Hex Nut Zinc Plated	Crown Bolt, Inc (Home Depot)	030699084401	2	9.57/100
1 Prices do not include shipping and handling if applicable. 2 Price is approximated based on information from various suppliers.				**Total: 36.02/ea (1,801.18)**

Table H2. Candle Insertion Tool (CIT) supply list.

Equipment/Tool	Manufacturer/Supplier	Model/SKU	Quantity	Price ($)[1]
6” Zinc Plated Catch Post Safety Hasp	Everbilt (Home Depot)	030699160761	2	7.49/ea
¼” -20 Nylon Lock Nut Zinc Plated	Crown Bolt, Inc (Home Depot)	030699192618	6	0.98/2
¼” x ¾” Hex Bolt Zinc Plated	Crown Bolt, Inc (Home Depot)	030699000364	6	0.10/ea
11/32” x 1 7/8” x 0.025” Extension Spring	Everbilt (Home Depot)	030699160860	1	3.38/4
7/16” x 2” Clevis Pin Zinc Plated	Crown Bolt, Inc (Home Depot)	030699880381	1	2.11
1 ½” Split Key Ring	Hillman (Home Depot)	736511590319	1	0.97/2
1/8” x ½” x 3’ Aluminum-Flat	SteelWorkS (Menards)	040395561960	1	3.57
3/16” Medium Aluminum Rivets	Arrow Fasteners Company, Inc (Home Depot)	RMA3/16IP 079055008309	1	4.96/100
1 Prices do not include shipping and handling if applicable.				**Total: 25.58**

Table H3. Candle Removal Tool (CRT) supply list.

Equipment/Tool	Manufacturer/Supplier	Model/SKU	Quantity	Price ($)[1]
3/8” x 4” Eye Bolt Zinc Plated with Hex Nut	Crown Bolt, Inc (Home Depot)	030699089864	1	0.81
3/8” -16 Nylon Lock Nut Zinc Plated	Crown Bolt, Inc (Home Depot)	030699192816	1	0.98/2
3/8” x 1 ½” Fender Washer Zinc Plated	Crown Bolt, Inc (Home Depot)	030699201204	2	0.24/ea
2” Non-Removable Pin Narrow Utility Hinges Zinc Plated	Everbilt (Home Depot)	030699151546	2	2.78/2
2” x 4” Angle Framing Anchor Zinc Plated	Simpson (Home Depot)	044315043000	2	2.98/ea
3/16” Medium Aluminum Rivets	Arrow Fasteners Company, Inc (Home Depot)	RMA3/16IP 079055008309	16	4.96/100
1/8” x ½” x 3’ Aluminum-Flat	SteelWorkS (Menards)	040395561960	1	3.57
1 Prices do not include shipping and handling if applicable.				**Total: 14.88**

Table H4. Tool Handling Equipment supply list.

Equipment/Tool	Manufacturer/Supplier	Model/SKU	Quantity	Price ($)[1]
3/8” x 100’ Diamond-Braid Poly Rope	Everbilt (Home Depot)	030699141562	1	8.97
¼” x 100’ Diamond-Braid Poly Rope with Cord Storage	Everbilt (Home Depot)	030699141142	1	7.47
¼” x 2 ½” Stainless Steel Spring Link	Lehigh (Home Depot)	071514005447	1	4.97
5/16” x 3 ¼” Stainless Steel Spring Link	Lehigh (Home Depot)	071514005454	1	6.29
Tangle Free Cord Storage “KORD-O-RAP”	Home Depot	693554912155	1	0.98
1 Prices do not include shipping and handling if applicable.				**Total: 28.68**